NASA/TM–2013-218056

Dependence of Dynamic Modeling Accuracy on Sensor Measurements, Mass Properties, and Aircraft Geometry

Jared A. Grauer and Eugene A. Morelli
Langley Research Center, Hampton, Virginia

November 2013

NASA STI Program . . . in Profile

Since its founding, NASA has been dedicated to the advancement of aeronautics and space science. The NASA scientific and technical information (STI) program plays a key part in helping NASA maintain this important role.

The NASA STI program operates under the auspices of the Agency Chief Information Officer. It collects, organizes, provides for archiving, and disseminates NASA's STI. The NASA STI program provides access to the NASA Aeronautics and Space Database and its public interface, the NASA Technical Report Server, thus providing one of the largest collections of aeronautical and space science STI in the world. Results are published in both non-NASA channels and by NASA in the NASA STI Report Series, which includes the following report types:

- TECHNICAL PUBLICATION. Reports of completed research or a major significant phase of research that present the results of NASA Programs and include extensive data or theoretical analysis. Includes compilations of significant scientific and technical data and information deemed to be of continuing reference value. NASA counterpart of peer-reviewed formal professional papers, but having less stringent limitations on manuscript length and extent of graphic presentations.

- TECHNICAL MEMORANDUM. Scientific and technical findings that are preliminary or of specialized interest, e.g., quick release reports, working papers, and bibliographies that contain minimal annotation. Does not contain extensive analysis.

- CONTRACTOR REPORT. Scientific and technical findings by NASA-sponsored contractors and grantees.

- CONFERENCE PUBLICATION. Collected papers from scientific and technical conferences, symposia, seminars, or other meetings sponsored or co-sponsored by NASA.

- SPECIAL PUBLICATION. Scientific, technical, or historical information from NASA programs, projects, and missions, often concerned with subjects having substantial public interest.

- TECHNICAL TRANSLATION. English-language translations of foreign scientific and technical material pertinent to NASA's mission.

Specialized services also include organizing and publishing research results, distributing specialized research announcements and feeds, providing information desk and personal search support, and enabling data exchange services.

For more information about the NASA STI program, see the following:

- Access the NASA STI program home page at *http://www.sti.nasa.gov*

- E-mail your question to help@sti.nasa.gov

- Fax your question to the NASA STI Information Desk at 443-757-5803

- Phone the NASA STI Information Desk at 443-757-5802

- Write to:
  STI Information Desk
  NASA Center for AeroSpace Information
  7115 Standard Drive
  Hanover, MD 21076-1320

NASA/TM–2013-218056

Dependence of Dynamic Modeling Accuracy on Sensor Measurements, Mass Properties, and Aircraft Geometry

Jared A. Grauer and Eugene A. Morelli
Langley Research Center, Hampton, Virginia

National Aeronautics and
Space Administration

Langley Research Center
Hampton, Virginia 23681-2199

November 2013

Available from:

NASA Center for AeroSpace Information
7115 Standard Drive
Hanover, MD 21076-1320
443-757-5802

Abstract

The NASA Generic Transport Model (GTM) nonlinear simulation was used to investigate the effects of errors in sensor measurements, mass properties, and aircraft geometry on the accuracy of identified parameters in mathematical models describing the flight dynamics and determined from flight data. Measurements from a typical flight condition and system identification maneuver were systematically and progressively deteriorated by introducing noise, resolution errors, and bias errors. The data were then used to estimate nondimensional stability and control derivatives within a Monte Carlo simulation. Based on these results, recommendations are provided for maximum allowable errors in sensor measurements, mass properties, and aircraft geometry to achieve desired levels of dynamic modeling accuracy. Results using additional flight conditions and parameter estimation methods, as well as a nonlinear flight simulation of the General Dynamics F-16 aircraft, were compared with these recommendations.

Contents

Nomenclature

Roman

A	multisine total amplitude [rad]
a_x, a_y, a_z	body frame translational acceleration [ft/s^2]
a_k	multisine amplitude [rad]
b	wingspan [ft]
C	nondimensional coefficient
$\bar{c}$	mean aerodynamic chord [ft]
$\mathbf{e}$	error vector
I	inertia [slug $\cdot$ ft^2]
$J(\boldsymbol{\theta})$	cost function
j	imaginary number, $\sqrt{-1}$
K	set of available excitation frequencies
M	total number of excitation frequencies
m	mass [slug]
N	number of data samples
p, q, r	body frame roll, pitch, yaw rates [rad/s]
$\bar{q}$	dynamic pressure [lbf/ft^2]
$\mathbf{R}$	noise covariance matrix
$\Re$	real part
S	wing area [ft^2]
T	data record length [s]
t	time [s]
V	airspeed [ft/s]
$\mathbf{X}$	regressor matrix
$\mathbf{y}$	model output
$\mathbf{z}$	measurement

Greek

α	angle of attack [rad]
β	sideslip angle [rad]
Δ	perturbation value
δ	control surface deflection [rad]
$\boldsymbol{\theta}$	parameter estimate vector
ρ	air density [slug/ft^3]
$\boldsymbol{\Sigma}(\boldsymbol{\theta})$	parameter estimate covariance matrix
σ	standard deviation
ϕ, θ, ψ	Euler roll, pitch, yaw angles [rad]
ϕ_k	multisine phase angle [rad]
ω	frequency [rad/s]

Superscripts

$\dot{}$	time derivative
†	complex conjugate transpose
$\hat{}$	estimated value
$^{-1}$	inverse

Subscripts

$_0$	trim value
$_a$	aileron

$_e$	elevator
$_l$, $_m$, $_n$	body frame roll, pitch, yaw moments
$_r$	rudder
$_X$, $_Y$, $_Z$	body frame longitudinal, side, heave forces
$_x$, $_y$, $_z$	body axis components

Acronyms

CAD	Computer-Aided Design
GTM	Generic Transport Model
NASA	National Aeronautics and Space Administration
RPF	Relative Peak Factor
SIDPAC	System IDentification Programs for AirCraft

1 Introduction

A routine goal of system identification, within the context of aircraft flight dynamics, is to estimate from experimental flight test data a set of nondimensional stability and control derivatives, and their uncertainties, within a linear system of differential equations. These results comprise a dynamic model of the aircraft, which then enables applications including performance and handling qualities analysis, aircraft redesign, flight simulator development, and control law synthesis. It is important to understand how errors in the flight test and system identification processes manifest in the parameter estimates to have confidence in the results and to adequately instrument the hardware. Failure to do so will lead to poorer system identification results that may require additional time and money to correct.

The consequences of incurring measurement noise, unmodeled dynamics, and information deficiency due to lack of excitation on system identification results are well understood [1–3]. Although not in common practice, methods were developed to identify models from quantized data [4, 5]. In the 1970's, studies [6–9] were conducted to determine the consequence of flight instrumentation errors on the aircraft stability and control derivative estimates, in dimensional form, using the output-error method in the time domain [1, 10] with linear simulation models and doublet excitation inputs. These works focused on time skews; filter lags; sensor position, misalignment, bias, and scale factor errors; and accelerometer and air flow angle correction errors. Because the estimates were in dimensional form, results were not valid for other flight conditions or for other aircraft. These studies were not able to take advantage of modern excitation input design and parameter estimation techniques, nor did they consider nondimensionalized stability and control derivatives, nor did they examine the effect of sensor resolution, mass and inertia errors, and geometry errors.

One sector of current research and development that could benefit from this information is the design of subscale, unmanned air vehicles. Although envisioned as cheaper alternatives to manned flight vehicles, these aircraft may become prohibitively expensive due to the cost of high quality onboard sensors that are also small and light weight. Understanding the trade offs between sensor quality and modeling accuracy helps designers create better aircraft system solutions faster and more cheaply. Mass distribution and aircraft geometry properties are found using intricate computer aided drawing (CAD) models or by experiment, both of which are time consuming processes that introduce error and must be repeated for new configurations. Designers would benefit from a set of guidelines and recommendations that relate the accuracy of these measurements to the accuracy of dynamic models identified from experimental flight test data.

This report presents such guidelines. Section 2 describes a high-fidelity, nonlinear simulation of a transport style aircraft, as well as a maneuver designed for system identification. Section 3 presents the model structure for the aerodynamic force and moment coefficients, and explains the equation-error method for estimating nondimensional stability and control derivatives in the frequency domain using experimental flight test data. In Section 4, increasing errors are sequentially introduced to each measurement while nondimensional stability and control derivatives are estimated and recorded within a Monte Carlo simulation. A summarizing table with recommendations to meet 2%, 5%, and 10% error budgets on the most important stability and control derivatives is presented. This table is the primary contribution of this paper and will give designers guidelines for selecting instrumentation and measurement accuracies. These recommendations are compared with additional flight conditions, parameter estimation methods, and aircraft simulations.

All of the input design, signal processing, and system identification work presented in this paper was done using software written in MATLAB® called System IDentification Programs for AirCraft (SIDPAC) [1], which was developed at NASA Langley Research Center and is continually being expanded and improved. SIDPAC has been applied successfully to a wide variety of flight and wind tunnel experiments at NASA Langley Research Center and

elsewhere, and is used at more than 80 institutions worldwide.

2 Materials

2.1 NASA Generic Transport Model

This work used the NASA Generic Transport Model (GTM), which is a nonlinear, rigid-body, flight dynamics simulation of a subscale, transport aircraft having mass and geometry parameters listed in Table 1. The GTM was selected for analysis because it is a high-fidelity, nonlinear simulation of a subscale aircraft. The GTM represents a conventional transport aircraft, having relatively well-known flight dynamics and behaviors. Additionally, the GTM was chosen because parameter estimation results can be compared to the true parameters determined using numerical linearization.

The GTM simulates the nonlinear, six degree of freedom, rigid body dynamics of the aircraft. Aerodynamic control surfaces include the elevator, aileron, rudder, spoilers, stabilizers, and flaps. The aerodynamic model used in the GTM is derived from a series of wind tunnel tests conducted at the NASA Langley Research Center [11]. A 5.5% scaled wind tunnel test article was used in the 14- by 22-Foot Subsonic Tunnel under static and forced oscillation testing to generate aerodynamic tables. These tables were augmented with data from rotary balance tests conducted using a 3.5% scaled wind tunnel test article in the 20-Foot Vertical Spin Tunnel. A polynomial-based aerodynamic model was then extracted from the data using multivariate orthogonal functions, expanded in the aircraft states and controls, and is implemented in the simulation [1, 12, 13]. The GTM also includes two turbojet engines, the dynamics for which are modeled as first order lags from the pilot throttle input to the thrust output. This model is based on multivariate orthogonal functions identified from ground testing, with additional ram drag corrections that vary with altitude and airspeed.

The GTM simulation software was written in MATLAB®. The user provides an initial state vector and a time history of control surface inputs. The simulation then computes time histories of the aircraft translational and rotational positions, velocities, and accelerations, as well as power and thrust states. Additional tools are provided to trim the aircraft and compute linear perturbation models about those trim conditions.

2.2 Reference Excitation Maneuver

Simulation data for a single reference flight maneuver were examined. For this maneuver, the GTM was trimmed for straight and level flight at a 1200 ft altitude and a 130 ft/s airspeed, which is a typical flight condition for this aircraft [14]. The simulation code determined trim values of +4.52 deg angle of attack, +1.40 deg elevator deflection, and 15% throttle for this condition.

Orthogonal phase-optimized multisine control input perturbations [1, 15] were chosen to excite the GTM for system identification. These multiple-axis inputs are commonly used for system identification at NASA Langley Research Center and have led to good modeling results in a variety of flight conditions including hypersonic, high sideslip stall, and post-stall flight, as well as normal flight conditions [15, 16]. Each of the elevator, aileron, and rudder control surface deflections had the form

$$\begin{aligned} \delta(t) &= \delta_0 + \Delta\delta(t) \\ &= \delta_0 + \sum_{k \in K} a_k \sin\left(\frac{2\pi k}{T} t + \phi_k\right) \end{aligned} \tag{1}$$

where δ_0 is the trim value, $\Delta\delta(t)$ is the perturbation, a_k is the amplitude, T is the excitation record length, ϕ_k is the phase angle, $\omega_k = 2\pi k/T$ is the excitation frequency, and K is the set of available frequencies for that input.

The excitation record length was chosen as $T = 35$ s, which corresponds to a fundamental frequency of 0.0286 Hz, to provide sufficient information content for system identification. Excitation frequencies were selected as integer multiples of this fundamental frequency and between the range 0.2 Hz and 2.0 Hz, where the rigid body dynamics of interest typically reside. Because the excitation frequencies are harmonic multiples of the fundamental frequency, the excitation inputs are mutually orthogonal and were excited simultaneously to shorten experiment durations without correlating data and deteriorating estimation results. Excitation frequencies were assigned to the inputs in an alternating manner so that each input has wide-band frequency content. For simplicity, amplitudes were selected to have uniform power and normalized such that the elevator, aileron, and rudder have perturbation amplitudes

$$A = a_k\sqrt{M} \tag{2}$$

of 2.0 deg, 0.5 deg, and 1.5 deg, respectively, where M is the number of frequencies used in the input. These amplitudes are typical of those used in practice [16]; smaller amplitudes result in lower signal-to-noise ratios and larger amplitudes can excite nonlinear motions. The phase angles were determined using a simplex search optimization to minimize the relative peak factors

$$\text{RPF} = \frac{\max[\Delta\delta(t)] - \min[\Delta\delta(t)]}{2\sqrt{2}\cdot\text{rms}[\Delta\delta(t)]} \tag{3}$$

of the inputs to keep the aircraft near the trim condition for linear modeling. These excitation inputs are parameterized in Table 2.

The GTM was simulated with these inputs at the reference flight condition and the resulting time history data is shown in Figure 1. Dynamic responses are small enough to remain within expected linear regimes and large enough so measurements are above realistic noise floors. Airspeed, air flow angles, and rotational velocity outputs are all within the regions of validity for the aerodynamic database [11].

3 Methods

3.1 Aerodynamic Models

Observing the conventional simplifying assumptions for a rigid body flight dynamics model of a fixed-wing aircraft [1, 17, 18], the nonlinear equations of motion can be rearranged to compute the nondimensional aerodynamic force and moment coefficients

$$\begin{aligned}
C_Y &= (ma_y)/(\bar{q}S) \\
C_Z &= (ma_z)/(\bar{q}S) \\
C_l &= [I_{xx}\dot{p} - I_{xz}(\dot{r} + pq) + (I_{zz} - I_{yy})qr]/(\bar{q}Sb) \\
C_m &= [I_{yy}\dot{q} + (I_{xx} - I_{zz})pr + I_{xz}(p^2 - r^2)]/(\bar{q}S\bar{c}) \\
C_n &= [I_{zz}\dot{r} - I_{xz}(\dot{p} - qr) + (I_{yy} - I_{xx})pq]/(\bar{q}Sb)
\end{aligned} \tag{4}$$

by substituting measured data on the right side of Equation 4 [1]. The longitudinal coefficient C_X is not included here because it is more closely associated with the slower phugoid mode and is often excluded from a control law design. The mass, inertia, wing reference area, mean aerodynamic chord, and wingspan of the aircraft are typically known before the flight test. Dynamic pressure, rotational velocities, and translational accelerations are

measured by onboard sensors. Angular velocity measurements are numerically smoothed and differentiated to compute angular accelerations [1].

The aerodynamic force and moment coefficients in Equation 4 were modeled in terms of the aircraft states and controls with the linear expansions [1, 17, 18]

$$\begin{aligned}
C_Y &= C_{Y_\beta}\Delta\beta + C_{Y_p}\frac{b\Delta p}{2V} + C_{Y_r}\frac{b\Delta r}{2V} + C_{Y_{\delta_a}}\Delta\delta_a + C_{Y_{\delta_r}}\Delta\delta_r \\
C_Z &= C_{Z_0} + C_{Z_\alpha}\Delta\alpha + C_{Z_q}\frac{\bar{c}\Delta q}{2V} + C_{Z_{\delta_e}}\Delta\delta_e \\
C_l &= C_{l_\beta}\Delta\beta + C_{l_p}\frac{b\Delta p}{2V} + C_{l_r}\frac{b\Delta r}{2V} + C_{l_{\delta_a}}\Delta\delta_a + C_{l_{\delta_r}}\Delta\delta_r \\
C_m &= C_{m_0} + C_{m_\alpha}\Delta\alpha + C_{m_q}\frac{\bar{c}\Delta q}{2V} + C_{m_{\delta_e}}\Delta\delta_e \\
C_n &= C_{n_\beta}\Delta\beta + C_{n_p}\frac{b\Delta p}{2V} + C_{n_r}\frac{b\Delta r}{2V} + C_{n_{\delta_a}}\Delta\delta_a + C_{n_{\delta_r}}\Delta\delta_r
\end{aligned} \tag{5}$$

which are valid for small deviations about the trim condition, where Δ indicates a perturbation. This is a commonly used aerodynamic model and application of step-wise regression [1] confirmed that this model is statistically appropriate for the reference flight maneuver data.

3.2 Equation-Error Parameter Estimation in the Frequency Domain

Given the measurements of the aerodynamic coefficients in Equation 4 and the model structure in Equation 5, it is a parameter estimation problem to determine the unknown nondimensional stability and control derivatives that best match the equations to the data. The equation-error method in the frequency domain [1] was used to estimate the stability and control derivatives. This method ignores sensor noise and modeling error at higher frequencies, has produced good results in practice, and provides an analytical solution amenable to Monte Carlo simulation.

The first step is to transform the data into the frequency domain using the Fourier transform. A measured signal $z(t)$ has the finite Fourier transform

$$z(j\omega) = \int_0^T z(t)e^{-j\omega t}dt \tag{6}$$

which, for relatively fast sampling frequencies, can be approximated by the discrete Fourier transform

$$z(j\omega_m) \simeq \Delta t \sum_{i=0}^{N-1} z(i\Delta t)e^{-j\omega_m i\Delta t} \tag{7}$$

where Δt is the sampling period and N is the number of data samples. A high-accuracy chirp-z transform with cubic polynomial interpolation [1, 19] was used to implement the Fourier transform using frequencies between 0.1 Hz and 2.5 Hz, in 0.025 Hz increments.

Each force and moment coefficient parameter estimation problem in Equation 5 was arranged into the least-squares framework as

$$\begin{aligned}
\mathbf{z} &= \mathbf{y} + \mathbf{e} \\
&= \mathbf{X}\boldsymbol{\theta} + \mathbf{e}
\end{aligned} \tag{8}$$

where $\mathbf{y}$ is the Fourier transform of the model output, $\mathbf{e}$ is the Fourier transform of the modeling error, $\mathbf{X}$ contains Fourier transforms of the explanatory variable time histories,

and $\boldsymbol{\theta}$ are the unknown nondimensional stability and control derivatives. Minimizing the least-squares cost function

$$J(\boldsymbol{\theta}) = \frac{1}{2}(\mathbf{z} - \mathbf{X}\boldsymbol{\theta})^{\dagger}(\mathbf{z} - \mathbf{X}\boldsymbol{\theta}) \tag{9}$$

where † denotes the complex conjugate transpose, results in the parameter estimates and associated uncertainties

$$\begin{aligned} \hat{\boldsymbol{\theta}} &= \left[\Re\{\mathbf{X}^{\dagger}\mathbf{X}\}\right]^{-1}\Re\{\mathbf{X}^{\dagger}\mathbf{z}\} \\ \hat{\boldsymbol{\Sigma}}(\hat{\boldsymbol{\theta}}) &= \hat{\sigma}^2\left[\Re\{\mathbf{X}^{\dagger}\mathbf{X}\}\right]^{-1} \end{aligned} \tag{10}$$

where the equation-error variance $\hat{\sigma}^2$ was estimated from the model residuals [1] and $\Re$ denotes the real part of a complex number. The bias terms C_{Z_0} and C_{m_0} cannot be estimated with frequency domain techniques because the data is detrended prior to analysis, but these terms are not used in a linear dynamics model.

3.3 Error Models

This section describes the mathematical models for the errors used to corrupt the measurements. The first type of error examined is due to quantization, which occurs when sensor measurements are converted into digital numbers. Quantization is an important issue in system identification because it changes the amplitude and frequency content of the data. This source of error remains a problem because although data systems can sample over a large range, system identification maneuvers are often designed to elicit small-amplitude responses that can be near the resolution floor of the avionics hardware. Errors due to quantization affect the computation of the aerodynamic coefficients in Equation 4 and the nondimensional stability and control derivatives in Equation 5. For a given measurement $z(t)$, the quantized measurement is

$$\text{quant}\{z(t)\} = \Delta_z \cdot \text{round}\left(\frac{z(t)}{\Delta_z}\right) \tag{11}$$

where Δ_z is the resolution of the measurement and round is a function that rounds the argument to the nearest integer. Figure 2 shows for example the progressive quantization of the angle of attack measurement from the reference excitation maneuver. The first plot is the original time history with added measurement noise. The next three plots show this measurement as the resolution Δ_α is degraded to 0.6 deg, 1.2 deg, and 1.8 deg.

The second source of error considered is bias error in the aircraft mass distribution and geometry parameters. The mass distribution of the aircraft can be measured experimentally using balancing and swinging techniques, or can be computed using CAD software. In either case, errors occur in determining the aircraft mass and the inertia tensor. Similarly, errors are incurred in the description of the aircraft geometry, namely the mean aerodynamic chord, the wingspan, and the wing reference area. These parameters are important because they affect the computations in Equation 4 and 5. For example, the pitch moment of inertia is modeled as $I_{yy} + \Delta_{I_{yy}}$, where $\Delta_{I_{yy}}$ is a constant, uniformly distributed bias.

Several error models were not considered in this report. While realistic noise sequences were applied to the data, the amplitude and statistical characteristics of the noise sequences were not varied because analytical and experimental results for describing the accuracy of estimated parameters using noisy data already exist [1–3]. Other studies [6,8,9] investigated the effects of bias and scale factor errors on sensor calibrations, as well as alignment, installation, and correction errors. In the frequency domain analysis used here, bias errors are all removed during detrending, before the Fourier transforms are applied, and are not a factor in the linear dynamic modeling. Scale factor errors manifest as multiplicative errors which

are directly proportional to the estimated stability and control derivatives. Finally, a study using output-error parameter estimation was already conducted to investigate the effects due to time skews between sensor measurements and signal-conditioning filter lags [7].

4 Results

This section presents the results of dynamic modeling accuracy dependence on sensors measurements, mass properties, and aircraft geometry. A baseline case is first presented, where nondimensional stability and control derivatives were estimated without corrupting the measurements, except for adding Gaussian white noise. Afterwards, errors were systematically introduced into the measurements to determine thresholds for meeting 2%, 5%, and 10% accuracies on the estimated parameters. Last, the analysis was repeated using different trim conditions, parameter estimation methods, and aircraft simulations to investigate sensitivities to these changes.

Monte Carlo simulations were used to produce the results. During investigation of the measurements of the aircraft mass properties or geometry, these values were first given a known random bias, distributed uniformly on a domain described by a percentage of the nominal value. Then measurements of the system outputs, for example the angle of attack and sideslip angle, were corrupted with a random Gaussian white noise sequence that implements a signal-to-noise ratio of 20:1, based on the root mean square of the variation in the data. The elevator, aileron, and rudder deflections were not corrupted with noise because these measurements are typically of high quality. During investigation of sensor measurements, the appropriate signals were then quantized. One thousand runs were performed for each level of accuracy and for each measurement corrupted. This number of runs was found to be beyond the amount needed for statistical convergence.

The estimated nondimensional stability and control derivatives diverged from the nominal estimates and exhibited increasing variation as the measurements were progressively corrupted. The damping derivatives, e.g. C_{n_r}, and off-axis derivatives, e.g. $C_{n_{\delta_a}}$, are less important in the dynamic model and are more difficult to estimate using system identification because the dynamic responses are smaller. Therefore, only the more important on-axis derivatives, e.g. $C_{n_{\delta_r}}$, are reported. Stability and control derivative estimates are plotted versus the accuracy level, as shown, for example, in Figure 4. Each point represents the mean value of the Monte Carlo simulations, using one thousand different measurement corruptions and noise sequences. The error bounds on each point represent the two standard deviation spread of the Monte Carlo simulations. The dashed lines represent the 10% variation of the finite difference results. Perturbations for computing numerical finite difference values were selected as the maximum deviations from the trim values in the flight data. Nondimensional stability and control derivatives computed using finite differences are listed in Table 3. Once any part of the two standard deviation interval crossed the 10% variation line for any of the reported on-axis stability and control derivatives, that level of accuracy was reported in Table 4 as the minimum needed to meet 10% error. For clarity, the 2% and 5% error bound levels are not shown in the plots, but those results are also listed in Table 4. This table, describing minimum accuracy levels for several measurements, is the main contribution of this work.

4.1 Nominal Estimation Results

Equation-error parameter estimation was used in the frequency domain with the reference flight data to estimate the nondimensional stability and control derivatives in the aerodynamic model. Figure 3(a) shows the model fits to the force and moment coefficients in the frequency domain, and Figure 3(b) shows the residuals, which are plotted at one tenth the

amplitude scale. The model fits had coefficients of determination above 0.99, the residuals had standard deviations two orders of magnitude less than the data, and estimated error bounds were all within 3.7% of the estimated model parameters. These metrics indicate that the model is appropriate for this set of data.

Nominal estimates of the nondimensional stability and control derivatives are provided in Table 3. The equation-error results were within two standard deviations of the finite difference results and thus were in statistical agreement. Differences between the results are mainly due to measurement noise and linearization effects. Table 3 also shows stability and control estimates using other methods of parameter estimation. Since all of these results are in statistical agreement, these results are consistent and there is sufficient information content in the data to identify accurate dynamics models.

4.2 Sensor Resolution Effects

This section discusses the effects of sensor quantization on the accuracy of dynamic models. Figures 4 through 11 illustrate the results and Table 4 contains the values at which the 2%, 5%, and 10% error criteria are violated.

When frequency domain equation-error parameter estimation is applied, resolution errors manifest as increased biases in the parameter estimates, shown in the figures as diverging oscillations. Although these results were obtained using Monte Carlo simulation with unique noise sequences, there is very little spread in the results, as indicated by the small error bounds, suggesting low sensitivity to varying random noise sequences at the noise level used here.

Overall, the longitudinal dynamics were more robust to quantization errors than the lateral/directional dynamics because the lateral/direction dynamics are more tightly coupled and contain more parameters to estimate. When one parameter begins to diverge, the other parameters become biased and also diverge. The damping derivatives depart first, followed by the control derivatives and then the static derivatives. Damping derivatives are typically the most difficult to estimate in aircraft system identification, whereas static derivatives are strong parameters and there is good excitation available for estimating the control derivatives.

The first measurements investigated were the angle of attack and sideslip angle, which are made with air flow vanes. These are important measurements because the aerodynamic forces and moments depend strongly on them. Corrections are often made for bias and scale factor calibrations, as well as offsets from the center of gravity. These measurements do not affect the aerodynamic coefficient calculations in Equation 4, but serve as explanatory variables in Equation 5. As the quantization level increases, making measurements of the angle of attack and sideslip angles progressively more coarse, the average values of the estimated stability and control derivatives from the Monte Carlo simulations diverge from the original values. The remainder of the linear nondimensional stability and control derivatives are shown in Figure 5 for completeness. As these are weaker parameters, they diverge sooner than the derivatives shown in Figure 4. Some of these parameters, for example $C_{n_{\delta_a}}$, violate the 10% error criterion even before quantization.

Gyroscopes measure the body-fixed rotational velocities. They are subject to bias errors and drifts, alignment errors, and effects due to structural flexibility of the aircraft. Gyroscope measurements and their derivatives are used in both the aerodynamic coefficients and the aerodynamic model. Figure 6 shows that the static terms C_{Y_β} and C_{Z_α} are relatively robust to gyroscope errors. In this case $C_{l_{\delta_a}}$ shows a particular sensitivity to measurement noise, as indicated by the larger spread in the Monte Carlo results.

Accelerometers measure the translational accelerations of the body and are subject to bias errors, position errors due to sensor offset from the center of mass, and alignment errors. Accelerometers only affect the computation of the aerodynamic force coefficients C_Y and

C_Z in Equation 4. Results are shown in Figure 7. The derivative $C_{Y_{\delta_r}}$ limits the resolution because the side acceleration is much smaller than the heave acceleration, as seen in the flight data in Figure 1.

Angle of attack and sideslip angle measurements can also be reconstructed when flying about trimmed flight conditions [20], such as the reference maneuver studied here. The differential equations

$$\begin{aligned} \dot{\beta} &\simeq \alpha p - r + (\sin\phi\cos\theta + a_y)/V \\ \dot{\alpha} &\simeq q - \beta p + (\cos\phi\cos\theta + a_z)/V \end{aligned} \tag{12}$$

may be integrated from initial conditions to reconstitute air flow angle measurements. While bias and drift errors accumulate during numerical integration of noisy data, these are removed prior to applying the Fourier transformation and do not affect the parameter estimates determined in the frequency domain. Figures 8 and 9 show nondimensional stability and control derivative estimates using reconstructed air flow angles and quantized gyroscope and accelerometer measurements, respectively. Corruption of the airspeed measurement in Equation 12 did not significantly deteriorate the estimates. For the stability and control derivatives under consideration, applying airflow angle reconstruction with degraded sensor resolutions quickly violated the error bound criterion due to additional biases and increases in the spread of the Monte Carlo simulation results. Here, not only are the rotational velocity and linear acceleration measurements degraded, but also the reconstructed air flow angle measurements. The lateral/directional derivatives were more susceptible than the longitudinal derivatives, and the air flow angle derivatives were more susceptible than the control derivatives. While stability and control derivative estimates were accurate, reconstructing air flow angle data relies on less information and is more susceptible to errors in this data, as previously noted [20].

Airspeed measurements are computed from pressure measurements, which are usually corrupted by bias and scale factor errors. Dynamic pressure measurements are used to nondimensionalize the aerodynamic coefficients. Figure 10 shows that after about 5 lbf/ft^2 quantization error in dynamic pressure, the parameter estimates diverge quickly. The limiting factor, $C_{Z_{\delta_e}}$, is the most sensitive because there is high excitation in the heave acceleration, and errors in the dynamic pressure magnify errors in the parameter estimation.

Control surface deflections are measured with potentiometers, and these are typically low in noise and correction errors. These measurements are of paramount importance in system identification, especially when using methods such as output-error that integrate the equations of motion using the input time histories. In the equation-error approach, these measurements only appear as explanatory variables in the aerodynamic model and the associated estimated model parameters have a reduced sensitivity to error. Figure 11 shows that the control derivative estimates diverge first as the quantization error in the control surface position measurement increases. After quantization at 1.4 deg, the contributions due to the aileron can no longer be deciphered.

It is important to note here that the error decreases with the square root of the number of data points. If time and money allowed for repeated testing at the same flight condition, additional data could help mitigate the effects of poor measurement resolution.

4.3 Mass and Geometry Bias Effects

This section discusses the effects on the dynamic model parameters due to errors in measuring the mass and geometry properties of the aircraft. Figures 12 through 14 illustrate the results and Table 4 contains the values at which the 2%, 5%, and 10% error criteria are violated.

Figures 12 through 14 show that mass and geometry errors do not change the mean value of the nondimensional stability and control derivative estimates and instead increase

the spread of the results. The longitudinal and lateral/directional derivatives are affected similarly, unlike the sensor quantization results. The static, damping, and control derivative uncertainties all grow at approximately the same rate. Due to some biases on the damping derivatives, these will surpass the error criteria quickly, and so the same set of on-axis static and control derivatives illustrated in Figure 4 were used to create Table 4.

Figure 12 shows the results for increasing errors in the aircraft mass and inertias, where the errors were modeled as uniformly distributed, random biases. In practice, these values are determined by CAD models and/or experimental techniques, and errors directly alter the aerodynamic coefficients. Errors would also affect center of mass corrections performed on many of the sensors, but this is not modeled here because the effects would be very small. There is essentially a one-to-one correspondence between the mass property error and the parameter estimation error; for example, 10% error in the mass quantities results in the two standard deviation spread of $C_{Z_{\delta_e}}$ surpassing the 10% error criterion. However, the values presented in Table 4 are less than this because parameter estimates are biased from the finite difference values.

The product of inertia I_{xz} is difficult to obtain accurately from experiments, but not a problem when using CAD modeling. Figure 13 was generated to address whether this quantity is needed for accurate dynamic modeling. The product of inertia I_{xz} only affects the C_l and C_n moment coefficients in Equation 4, and while it did not increase the rate of growth of the error bounds of the estimated parameters, it led to larger differences between the Monte Carlo and finite difference results, which in turn led to lower error requirements for meeting the same error criteria.

Figure 14 shows the results when corrupting the aircraft geometry measurements, which are either measured directly or computed using CAD programs. These values nondimensionalize the aerodynamic coefficients and appear in the nondimensional rate terms in the aerodynamic model. Errors impact the moment coefficients more than the force coefficients because the wing reference area is multiplied by either the mean aerodynamic chord or the wing span, thereby magnifying the error.

4.4 Additional Flight Conditions

The previous analysis was performed on the GTM nonlinear flight simulation for one single maneuver. To investigate how the measurement recommendations might change with the flight condition, the analysis was repeated for trim angles of attack between 0 deg and 10 deg, as described in Table 5. The same input sequence described in Table 2 was applied to the GTM in each trim condition. As the trim angle of attack increased and the trim airspeed decreased, the perturbations in the angle of attack increased while the rotational velocities became smaller. All flight data remained within the regime of validity for the GTM simulation.

Figure 15 shows estimation results for the pitching moment derivatives as the gyroscope resolution is progressively degraded, for several trim conditions. The 10% error criteria is based on the finite difference values listed in Table 5. At 0 deg angle of attack, these values are surpassed sooner because additional biases exist in the estimated parameters, perhaps due to the larger excursions from trim experienced. As the trim angle of attack increases, the manner in which the estimated stability and control derivatives diverge remains the same, and the values at which the error criteria are violated remain consistent. Therefore, the recommendations provided in Table 4 are independent of the flight condition, for straight and level flight below stall. If the model structure in Equation 5 changes, for example with unusual aircraft configurations or trim conditions, then these values would have to be determined again.

4.5 Additional Parameter Estimation Methods

The previous results employed the equation-error method in the frequency domain. Another common method for parameter estimation is to apply equation-error in the time domain. The same procedure is used, except that the Fourier transform in Equation 7 is not applied. While this process still retains the analytical solution, there are several disadvantages to the time domain analysis. For instance, more data points are used, resulting in longer computation times. There is no automatic filtering of frequency content away from the rigid body dynamics of interest, so higher frequency content such as noise and unmodeled dynamics must first be filtered. Time-domain residuals are typically colored, so that the estimated parameter error bounds must be corrected [1].

Results for degrading air flow angle measurements for the GTM reference maneuver are shown in Figure 16 using equation-error method in the time domain. The on-axis parameters diverged much faster than using the equation-error method in the frequency domain. The spread of some parameters including C_{l_β} and $C_{l_{\delta_a}}$ violate the 10% error criteria even with no quantization, due to the added noise on the measurements.

Another popular method of parameter estimation is the output-error method in the time domain [1, 10]. In this approach, a nonlinear optimization is used to iteratively find the stability and control derivatives that best match the model outputs to the experimental data. Equations 14 through 17 describe the equations of motion for the longitudinal and lateral/directional variables, as well as the model outputs. Again, the phugoid mode was not modeled. The output-error method integrates these equations from initial conditions using the time history of the inputs to obtain the outputs. The stability and control derivatives are then optimized so that the model outputs best match the measured outputs according to the cost function

$$J(\boldsymbol{\theta}) = \frac{1}{2}(\mathbf{z} - \mathbf{y})^T \hat{\mathbf{R}}^{-1}(\mathbf{z} - \mathbf{y}) \tag{13}$$

where $\mathbf{R}$ is the noise covariance matrix.

The results of using output-error estimation in the time domain for the GTM reference maneuver and air flow angle quantization are shown in Figure 17. The output-error method worked very well in the case of the C_Z and C_m coefficients. However as the quantization increased up to 1 deg, the estimates of the lateral derivatives quickly degraded. The lateral/directional dynamics are more coupled and there are more parameters to estimate, which degraded sooner than using the frequency domain equation-error method. For the case of quantized input measurements, the output-error method performed particularly poorly because of the numerical integration involved, consistent with previous research.

4.6 F-16 Nonlinear Simulation

A nonlinear simulation of the General Dynamics F-16 fighter aircraft was also used to check if results change with the aircraft size. The F-16 is a piloted, full-scale, fighter aircraft with properties listed in Table 1. The nonlinear simulation is a MATLAB® implementation [1] of the FORTRAN simulation presented by Stevens and Lewis [18], which utilizes modified aerodynamic tables from wind tunnel tests and engine dynamics identified from ground tests [21].

The F-16 simulation was trimmed at 10,000 ft altitude, with an airspeed of 450 ft/s and a 5 deg angle of attack. Perturbation inputs described in Table 2 were super-imposed on trim settings for the nonlinear F-16 simulation.

Parameter estimation results using equation-error in the frequency domain were similar to those found using the GTM. A representative case, showing parameter estimates with varying mass and inertia accuracy, is shown in Figure 18, exhibiting similar trends for varying flight conditions. The use of nondimensional stability and control derivatives and

Longitudinal equations:

$$\begin{bmatrix} \Delta\dot{\alpha} \\ \Delta\dot{q} \end{bmatrix} = \begin{bmatrix} \frac{\bar{q}_0 S\bar{c}}{mV_0} C_{Z_\alpha} + \frac{g\sin\alpha_0}{V_0} - \frac{T_0\cos\alpha_0}{mV_0} & 1 + \frac{\bar{q}_0 S\bar{c}}{2mV_0^2}\cos\alpha_0 C_{Z_q} \\ \frac{\bar{q}_0 S\bar{c}}{I_{yy}} C_{m_\alpha} & \frac{\bar{q}_0 S\bar{c}^2}{2V_0 I_{yy}} C_{m_q} \end{bmatrix} \begin{bmatrix} \Delta\alpha \\ \Delta q \end{bmatrix} + \begin{bmatrix} \frac{\bar{q}_0 S}{mV_0} C_{Z_{\delta_e}} \\ \frac{\bar{q}_0 S\bar{c}}{I_{yy}} C_{m_{\delta_e}} \end{bmatrix} \Delta\delta_e \tag{14}$$

$$\begin{bmatrix} \Delta\alpha \\ \Delta q \\ \Delta a_z \end{bmatrix} = \begin{bmatrix} 1 & 0 \\ 0 & 1 \\ \frac{\bar{q}S}{mg} C_{Z_\alpha} & \frac{\bar{q}S\bar{c}}{2V_0 mg} C_{Z_q} \end{bmatrix} \begin{bmatrix} \Delta\alpha \\ \Delta q \end{bmatrix} + \begin{bmatrix} 0 \\ 0 \\ \frac{\bar{q}S}{mg} C_{Z_{\delta_e}} \end{bmatrix} \Delta\delta_e \tag{15}$$

Lateral equations:

$$\begin{bmatrix} 1 & 0 & 0 & 0 \\ 0 & I_{xx} & -I_{xz} & 0 \\ 0 & -I_{xz} & I_{zz} & 0 \\ 0 & 0 & 0 & 1 \end{bmatrix} \begin{bmatrix} \Delta\dot{\beta} \\ \Delta\dot{p} \\ \Delta\dot{r} \\ \Delta\dot{\phi} \end{bmatrix} = \begin{bmatrix} \frac{\bar{q}S}{mV_0} C_{Y_\beta} & \frac{\bar{q}Sb}{2mV_0^2} C_{Y_p} + \sin\alpha_0 & \frac{\bar{q}Sb}{2mV_0^2} C_{Y_r} - \cos\alpha_0 & \frac{g\cos\theta_0}{V_0} \\ \bar{q}SbC_{l_\beta} & \frac{\bar{q}Sb^2}{2V_0} C_{l_p} & \frac{\bar{q}Sb^2}{2V_0} C_{l_r} & 0 \\ \bar{q}SbC_{n_\beta} & \frac{\bar{q}Sb^2}{2V_0} C_{n_p} & \frac{\bar{q}Sb^2}{2V_0} C_{n_r} & 0 \\ 0 & 1 & \tan\theta_0 & 0 \end{bmatrix} \begin{bmatrix} \Delta\beta \\ \Delta p \\ \Delta r \\ \Delta\phi \end{bmatrix} + \begin{bmatrix} \frac{\bar{q}S}{mV_0} C_{Y_{\delta_a}} & \frac{\bar{q}S}{mV_0} C_{Y_{\delta_r}} \\ \bar{q}SbC_{l_{\delta_a}} & \bar{q}SbC_{l_{\delta_r}} \\ \bar{q}SbC_{n_{\delta_a}} & \bar{q}SbC_{n_{\delta_r}} \\ 0 & 0 \end{bmatrix} \begin{bmatrix} \Delta\delta_a \\ \Delta\delta_r \end{bmatrix} \tag{16}$$

$$\begin{bmatrix} \Delta\beta \\ \Delta p \\ \Delta r \\ \Delta\phi \\ \Delta a_y \end{bmatrix} = \begin{bmatrix} 1 & 0 & 0 & 0 \\ 0 & 1 & 0 & 0 \\ 0 & 0 & 1 & 0 \\ 0 & 0 & 0 & 1 \\ \frac{\bar{q}S}{mg} C_{Y_\beta} & \frac{\bar{q}Sb}{2V_0 mg} C_{Y_p} & \frac{\bar{q}Sb}{2V_0 mg} C_{Y_r} & 0 \end{bmatrix} \begin{bmatrix} \Delta\beta \\ \Delta p \\ \Delta r \\ \Delta\phi \end{bmatrix} + \begin{bmatrix} 0 & 0 \\ 0 & 0 \\ 0 & 0 \\ 0 & 0 \\ \frac{\bar{q}S}{mg} C_{Y_{\delta_a}} & \frac{\bar{q}S}{mg} C_{Y_{\delta_r}} \end{bmatrix} \begin{bmatrix} \Delta\delta_a \\ \Delta\delta_r \end{bmatrix} \tag{17}$$

percent errors allow recommendations in Table 4 to be applicable to other aircraft. This is expected because the nondimensional stability and control derivatives remove the known dependence on aircraft mass and geometry properties.

5 Conclusions

This report investigated the effects of errors in sensor measurements, mass properties, and aircraft geometry on the accuracy of dynamic model parameters estimated from experimental flight test data. The NASA GTM nonlinear simulation was excited using orthogonal phase-optimized multisine perturbations on the elevator, aileron, and rudder inputs while in trimmed flight. Each case was run one thousand times using unique noise sequences, and the equation-error method was applied in the frequency domain to estimate longitudinal and lateral/directional nondimensional stability and control derivatives.

The findings and contributions of this report are:

1. A list of recommended measurement resolutions needed to meet 2%, 5%, and 10% errors budgets on estimated nondimensional stability and control derivatives using equation-error in the frequency domain are provided in Table 4.

2. Estimates of stability and control derivatives can be obtained by reconstructing angle of attack and sideslip angle measurements from gyroscopes and accelerometers; however, these sensors require better resolution in this case, especially the gyroscopes. Nonetheless, this method appears to be a viable alternative to using air flow angle vanes for system identification, as these sensors disturb the flow, add cost and complexity to the aircraft, and are difficult to calibrate.

3. The product of inertia I_{xz} was found to have a small impact on stability and control derivative estimates for typical fuselage-heavy aircraft. Here, this quantity can be safely approximated or neglected to save time and money if aircraft mass distributions are being determined experimentally, assuming small perturbation flight tests starting from wings-level flight conditions at relatively low angles of attack.

4. Repeated analysis showed that the results listed in Table 4 were not sensitive to variations in trim conditions below stall.

5. Equation-error parameter estimation in the frequency domain produces better results than in the time domain, due to noise sensitivities and unmodeled dynamics. Except for quantized control surface deflections, the output-error method produced excellent results up to a certain threshold, when large biases and standard deviations were incurred.

6. Results in Table 4 were found to scale with vehicle size, per analysis using an F-16 simulation.

References

1. Klein, V.; and Morelli, E.: *Aircraft System Identification: Theory and Practice*. AIAA Education Series, AIAA, 2006.

2. Ljung, L.: *System Identification: Theory for the User*. Information and System Sciences Series, Prentice Hall, Upper Saddle River, NJ, 2nd ed., 1999.

3. Morelli, E.; and Smith, M.: Real-Time Dynamic Modeling: Data Information Requirements and Flight Test Results. *Journal of Aircraft*, vol. 46, no. 6, Nov.–Dec. 2009, pp. 1894–1905.

4. Wang, L.; Yin, G.; Zhang, J.; and Zhao, Y.: *System Identification with Quantized Observations*. Springer, 2010.

5. Konishi, K.; and Kato, H.: A System Identification Method With Roughly Quantized Data Using Semidefinite Programming. Industrial Electronics Conference, IEEE, 2009, pp. 1426–1431.

6. Sorenson, J.: Analysis of Instrument Error Effects on the Identification Accuracy of Aircraft Parameters. TN-D-7830, NASA, Washington D.C., May 1972.

7. Steers, S.; and Illif, K.: Effects of Time-Shifted Data on Flight-Determined Stability and Control Derivatives. TN–D–7830, NASA, Washington, D.C., March 1975.

8. Hodge, W.; and Bryant, W.: Monte Carlo Analysis of Innacuracies in Estimated Aircraft Parameters Caused by Unmodeled Flight Instrumentation Errors. TN-D-7712, NASA, Washington D.C., February 1975.

9. Sorenson, J.; Mohr, R.; and Cline, T.: Instrumentation Requirements for Aircraft Parameter Identification with Application to the Helicopter. CR-132675, NASA, Washington D.C., June 1975.

10. Maine, R.; and Iliff, K.: Application of Parameter Estimation to Aircraft Stability and Control: The Output-Error Approach. Reference Publication 1168, NASA, June 1986.

11. Murch, A.; and Foster, J.: Recent NASA Research on Aerodynamic Modeling of Post-Stall and Spin Dynamics of Large Transport Aircraft. No. 2007–463 in 45th AIAA Aerospace Sciences Meeting and Exhibit, AIAA, Reno, NV, January 2007.

12. Morelli, E.: Global Nonlinear Aerodynamic Modeling using Multivariate Orthogonal Functions. *Journal of Aircraft*, vol. 32, no. 2, March–April 1995, pp. 270–277.

13. Morelli, E.; and DeLoach, R.: Wind Tunnel Database Development using Modern Experiment Design and Multivariate Orthgonal Functions. No. 2003–653 in 41st AIAA Aerospace Sciences Meeting and Exhibit, AIAA, Reno, NV, January 2003.

14. Jordan, T.; Foster, J.; Bailey, R.; and Belcastro, C.: AirSTAR: a UAV Platform for Flight Dynamics Control System Testing. No. 2006–3307 in Aerodynamic Measurement Technology and Ground Testing Conference, AIAA, San Francisco, CA, June 2006.

15. Morelli, E.: Flight-Test Experiment Design for Characterizing Stability and Control of Hypersonic Vehicles. *Journal of Guidance, Control, and Dynamics*, vol. 32, no. 3, May–June 2009, pp. 949–959.

16. Morelli, E.: Flight Test Maneuvers for Efficient Aerodynamic Modeling. No. 2011–6672 in AIAA Atmospheric Flight Mechanics Conference, AIAA, Portland, OR, August 2011.

17. McRuer, D.; Ashkenas, I.; and Graham, D.: *Aircraft Dynamics and Automatic Control*. Princeton Universtiy Press, 1973.

18. Stevens, B.; and Lewis, F.: *Aircraft Control and Simulation*. Wiley, 1992.

19. Morelli, E.: High Accuracy Evaluation of the Finite Fourier Transform Using Sampled Data. TM-110340, NASA, Hampton, VA, June 1997.

20. Morelli, E.: Real-Time Aerodynamic Parameter Estimation Without Air Flow Angle Measurements. *Journal of Aircraft*, vol. 49, no. 4, July-August 2012, pp. 1064–1074.

21. Nguyen, L.; Ogburn, M.; Gilbert, W.; Kibler, K.; Brown, P.; and Deal, P.: Simulation Study of Stall/Post-Stall Characteristics of a Fighter Airplane with Relaxed Longitudinal Static Stability. Technical Report TP 1538, NASA, 1979.

Tables

Table 1. Mass and geometry values used in aircraft simulations

Parameter	Symbol	GTM	F-16	Units
center of mass position	x_{cg}	0.25	0.25	$\%\bar{c}$
mean aerodynamic chord	$\bar{c}$	0.9153	11.320	ft
wing span	b	6.8488	30.000	ft
wing reference area	S	5.9018	300.00	ft^2
mass	m	1.5416	637.16	slug
roll inertia	I_{xx}	1.3270	9496.0	$slug{\cdot}ft^2$
pitch inertia	I_{yy}	4.2540	55814	$slug{\cdot}ft^2$
yaw inertia	I_{zz}	5.4540	63100.	$slug{\cdot}ft^2$
roll/yaw coupling inertia	I_{xz}	0.1200	982.00	$slug{\cdot}ft^2$

Table 2. Orthogonal phase-optimized multisine input description (record length $T = 35$ s)

Elevator			Aileron			Rudder		
$A = 2.0$ deg $a_k = 0.6667$ deg $M = 22$ RPF = 1.2445			$A = 0.5$ deg $a_k = 0.1091$ deg $M = 21$ RPF = 1.2136			$A = 1.5$ deg $a_k = 0.3273$ deg $M = 21$ RPF = 1.0658		
Index k	Frequency k/T [Hz]	Phase ϕ_k [rad]	Index k	Frequency k/T [Hz]	Phase ϕ_k [rad]	Index k	Frequency k/T [Hz]	Phase ϕ_k [rad]
7	0.2000	3.6221	8	0.2286	3.9280	9	0.2571	5.8733
10	0.2857	4.1272	11	0.3143	6.0649	12	0.3429	4.9406
13	0.3714	3.2037	14	0.4000	0.8306	15	0.4286	3.1968
16	0.4571	2.6584	17	0.4857	1.5477	18	0.5143	0.0323
19	0.5429	0.0811	20	0.5714	2.2952	21	0.6000	3.3582
22	0.6286	2.5869	23	0.6571	1.4435	24	0.6857	4.3454
25	0.7143	6.0820	26	0.7429	6.2755	27	0.7714	3.9451
28	0.8000	0.0769	29	0.8286	3.1900	30	0.8571	5.7802
31	0.8857	1.6735	32	0.9143	0.0810	33	0.9429	4.4729
34	0.9714	1.7690	35	1.0000	2.0319	36	1.0286	3.3028
37	1.0571	0.6256	38	1.0857	3.0491	39	1.1143	0.0384
40	1.1429	5.0289	41	1.1714	3.8835	42	1.2000	3.6866
43	1.2286	2.5389	44	1.2571	2.3799	45	1.2857	4.8036
46	1.3143	5.3888	47	1.3429	1.6406	48	1.3714	0.3270
49	1.4000	0.8353	50	1.4286	5.3963	51	1.4571	0.8943
52	1.4857	0.6303	53	1.5143	2.3521	54	1.5429	1.1219
55	1.5714	2.2350	56	1.6000	5.2871	57	1.6286	5.7885
58	1.6571	2.3720	59	1.6857	1.8165	60	1.7143	3.7299
61	1.7429	0.9076	62	1.7714	1.7858	63	1.8000	5.4749
64	1.8286	5.1943	65	1.8571	0.6440	66	1.8857	2.8322
67	1.9143	1.2656	68	1.9429	5.5245	69	1.9714	3.7967
70	2.0000	3.4607						

Table 3. Nondimensional stability and control derivative estimates for the GTM ($h_0 = 1200$ ft, $V_0 = 130$ ft/s, $\alpha_0 = 4.52$ deg)

Parameter	Numerical Central Finite Difference θ	Frequency Domain Equation-Error $\hat{\theta} \pm \hat{\sigma}(\hat{\theta})$	Time Domain Equation-Error $\hat{\theta} \pm \hat{\sigma}(\hat{\theta})$	Time Domain Output-Error $\hat{\theta} \pm \hat{\sigma}(\hat{\theta})$
C_{Y_β}	-1.0125	-1.0065 ± 0.0037	-1.0066 ± 0.0022	-1.0084 ± 0.0124
C_{Y_p}	$+0.0543$	$+0.0735 \pm 0.0158$	$+0.0727 \pm 0.0095$	$+0.0903 \pm 0.0553$
C_{Y_r}	$+0.8574$	$+0.8877 \pm 0.0238$	$+0.8863 \pm 0.0139$	$+0.9548 \pm 0.0761$
$C_{Y_{\delta_a}}$	-0.0177	-0.0155 ± 0.0032	-0.0156 ± 0.0020	-0.0315 ± 0.0136
$C_{Y_{\delta_r}}$	$+0.3387$	$+0.3390 \pm 0.0012$	$+0.3390 \pm 0.0006$	$+0.3446 \pm 0.0027$
C_{Z_α}	-4.8370	-4.8345 ± 0.0077	-4.8344 ± 0.0040	-4.8932 ± 0.0179
C_{Z_q}	-27.102	-27.609 ± 0.5040	-27.590 ± 0.2823	-28.735 ± 0.9357
$C_{Z_{\delta_e}}$	-0.4807	-0.4801 ± 0.0093	-0.4799 ± 0.0052	-0.4540 ± 0.0187
C_{l_β}	-0.1432	-0.1393 ± 0.0029	-0.1396 ± 0.0017	-0.1393 ± 0.0021
C_{l_p}	-0.3542	-0.3333 ± 0.0123	-0.3342 ± 0.0073	-0.3322 ± 0.0096
C_{l_r}	$+0.1331$	$+0.1535 \pm 0.0186$	$+0.1518 \pm 0.0110$	$+0.1645 \pm 0.0140$
$C_{l_{\delta_a}}$	-0.0760	-0.0735 ± 0.0025	-0.0736 ± 0.0015	-0.0722 ± 0.0024
$C_{l_{\delta_r}}$	$+0.0290$	$+0.0293 \pm 0.0009$	$+0.0293 \pm 0.0005$	$+0.0291 \pm 0.0006$
C_{m_α}	-1.6349	-1.6134 ± 0.0068	-1.6129 ± 0.0051	-1.6241 ± 0.0053
C_{m_q}	-41.215	-41.292 ± 0.4441	-41.301 ± 0.3319	-42.008 ± 0.3408
$C_{m_{\delta_e}}$	-1.7744	-1.7924 ± 0.0082	-1.7925 ± 0.0061	-1.8238 ± 0.0061
C_{n_β}	$+0.2165$	$+0.2147 \pm 0.0009$	$+0.2150 \pm 0.0006$	$+0.2180 \pm 0.0023$
C_{n_p}	-0.0408	-0.0461 ± 0.0039	-0.0449 ± 0.0024	-0.0366 ± 0.0106
C_{n_r}	-0.3840	-0.3892 ± 0.0059	-0.3875 ± 0.0037	-0.3796 ± 0.0159
$C_{n_{\delta_a}}$	-0.0025	-0.0032 ± 0.0008	-0.0031 ± 0.0005	$+0.0027 \pm 0.0025$
$C_{n_{\delta_r}}$	-0.1691	-0.1692 ± 0.0003	-0.1691 ± 0.0002	-0.1704 ± 0.0005

Table 4. Recommended measurement resolutions for achieving specified error budgets

Measurement	Symbol	2%	5%	10%	Units
Air Flow Angles	α, β	0.1014	0.2024	0.4048	deg
Dynamic Pressure	$\bar{q}$	0.0089	0.1446	2.2406	lbf/ft^2
Gyroscopes	p, q, r	1.8707	4.2064	5.5439	deg/s
Accelerometers	a_x, a_y, a_z	0.0127	0.0262	0.0524	g
Potentiometers	δ_e, δ_a, δ_r	0.0389	0.2457	0.4526	deg
Mass Distribution	m, I_{xx}, I_{yy}, I_{zz}, I_{xz}	0.0057	0.1858	4.1271	%
Mass Distribution	m, I_{xx}, I_{yy}, I_{zz}, $I_{xz} = 0$	0.1798	1.0323	1.4596	%
Aircraft Geometry	$\bar{c}$, b, S	0.2684	1.4223	3.0958	%

Table 5. Additional GTM trim conditions ($h_0 = 1200$ ft) and finite difference values

α_0 [deg]	V_0 [ft/s]	δ_{t_0}	δ_{e_0} [deg]	C_{m_α}	C_{m_q}	$C_{m_{\delta_e}}$
0	338.33	0.72	+5.19	-1.6437	-44.889	-1.8122
2	177.10	0.24	+3.56	-1.5378	-43.258	-1.7993
4	136.42	0.15	+1.84	-1.6211	-41.628	-1.7750
6	115.51	0.17	+0.18	-1.4117	-40.027	-1.8237
8	102.39	0.15	-1.00	-0.9992	-38.425	-1.8550
10	092.97	0.14	-1.79	-0.8814	-31.095	-1.8230

Figures

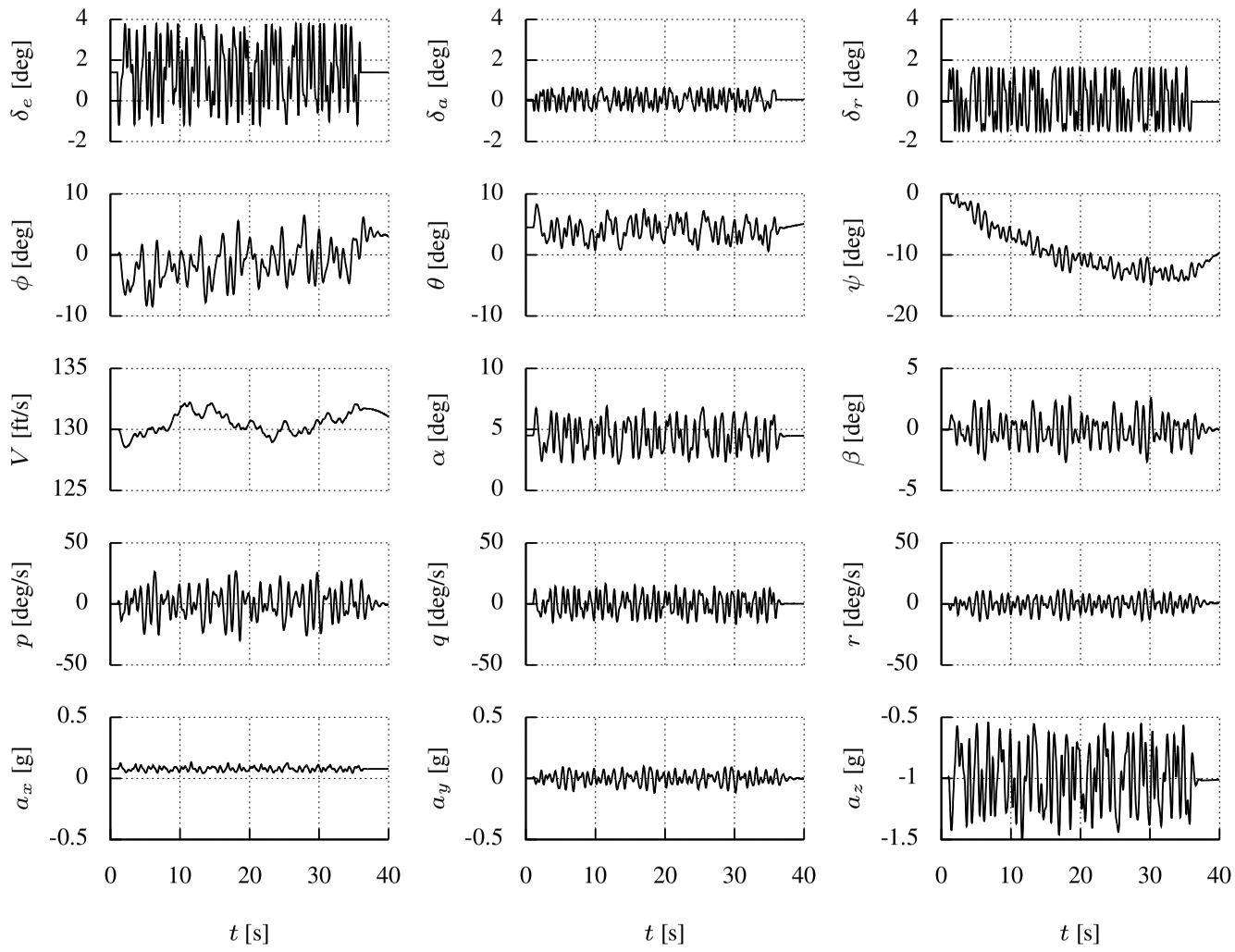

Figure 1. GTM reference maneuver simulation data

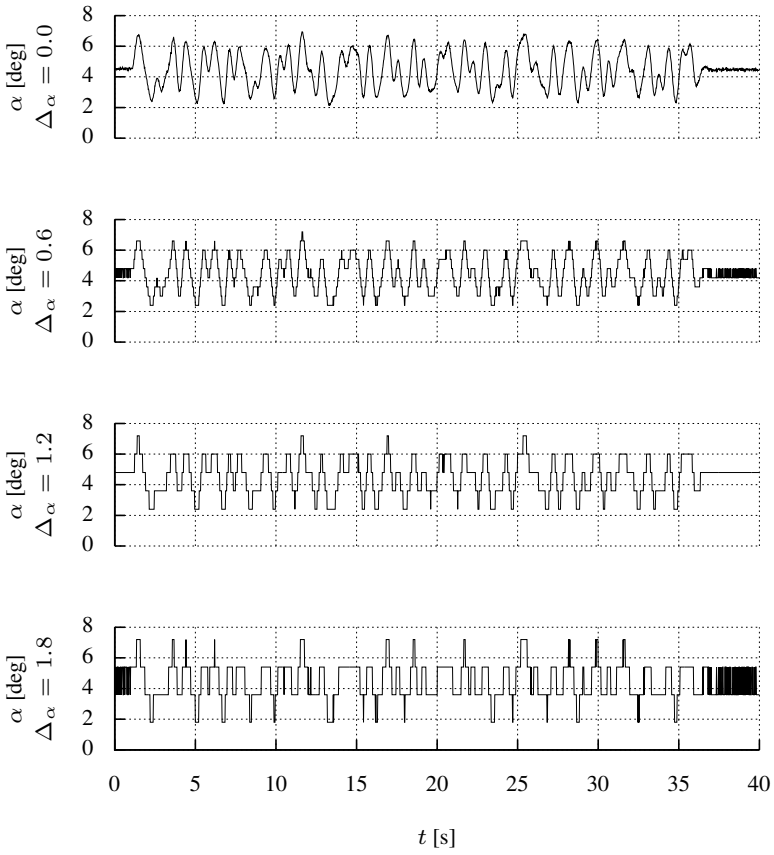

Figure 2. Noisy angle of attack measurement with progressive quantization

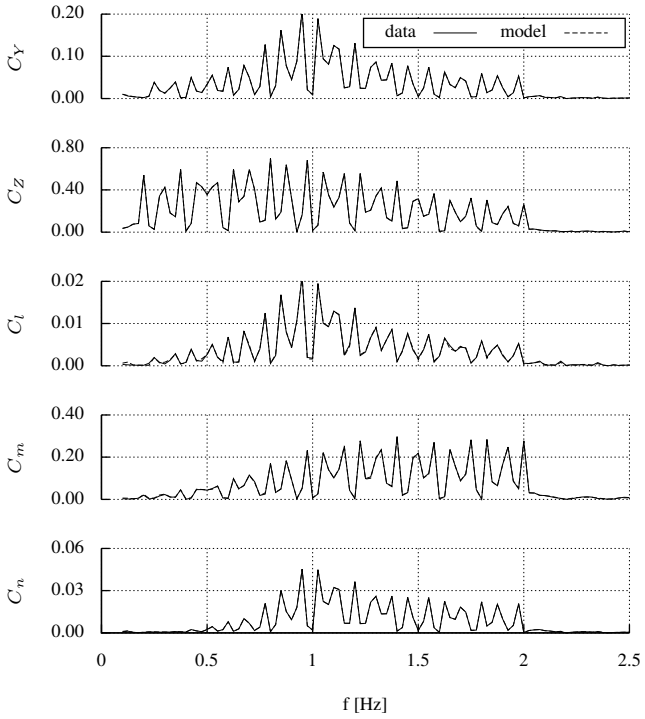

(a) computed and modeled aerodynamic force and moment coefficients

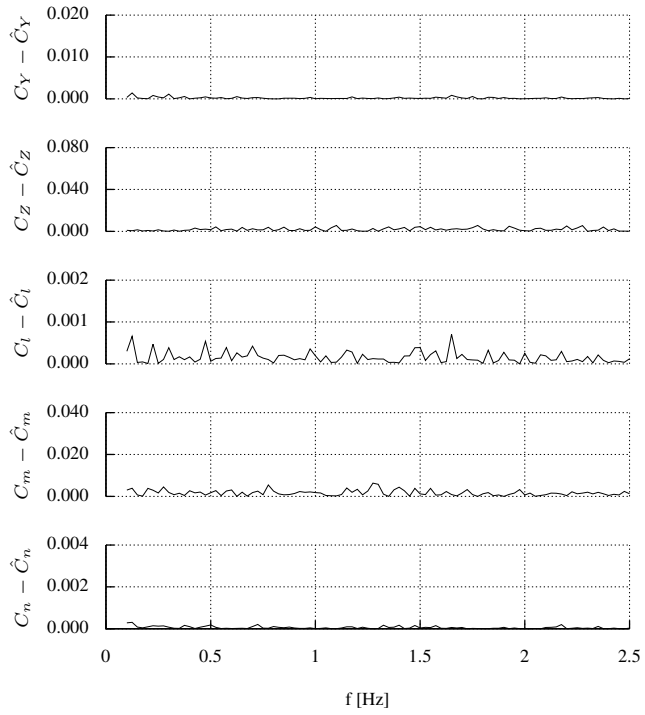

(b) residuals

Figure 3. Frequency domain data modeling for the GTM reference excitation maneuver

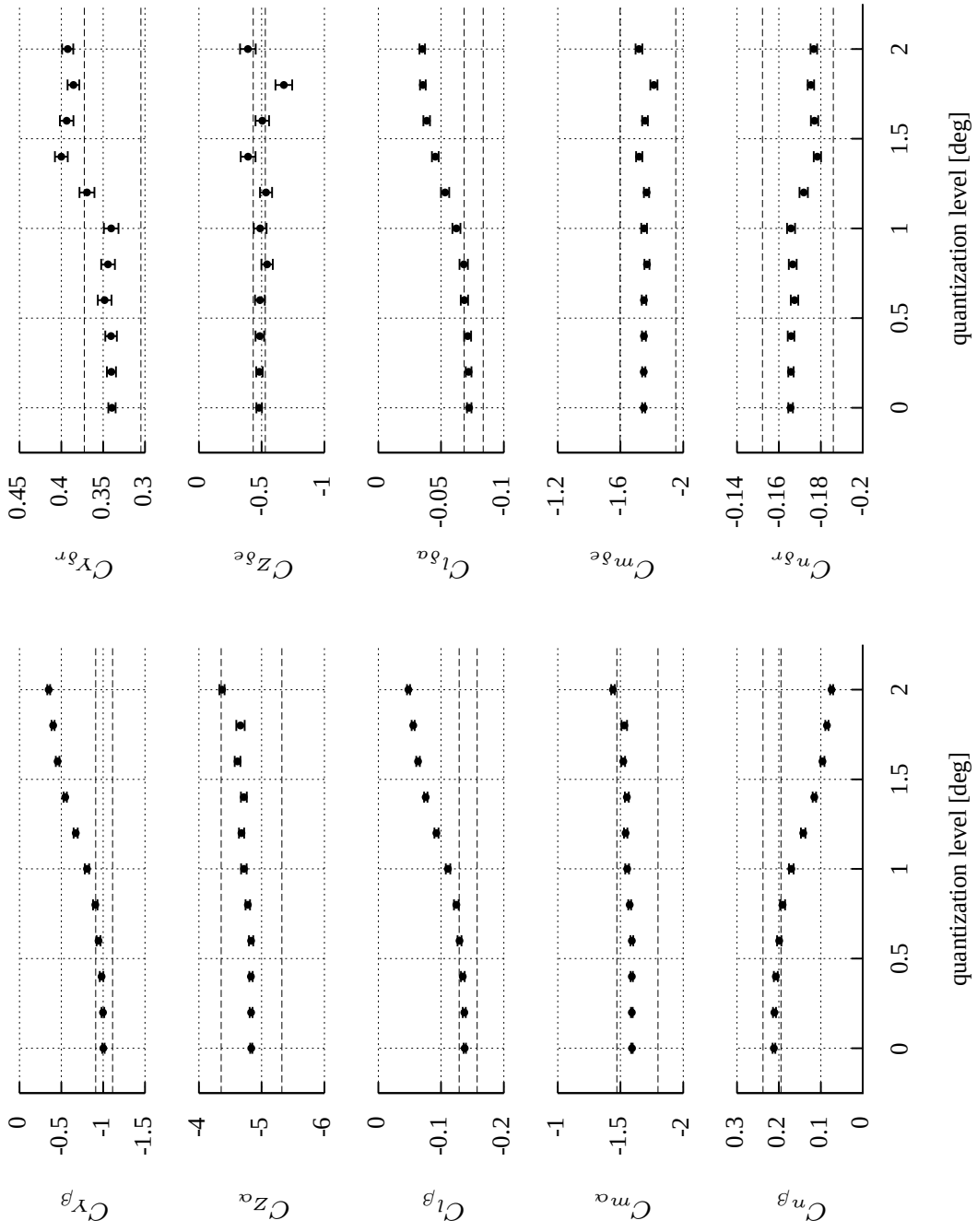

Figure 4. Variation in GTM stability and control derivatives with air flow angle resolution

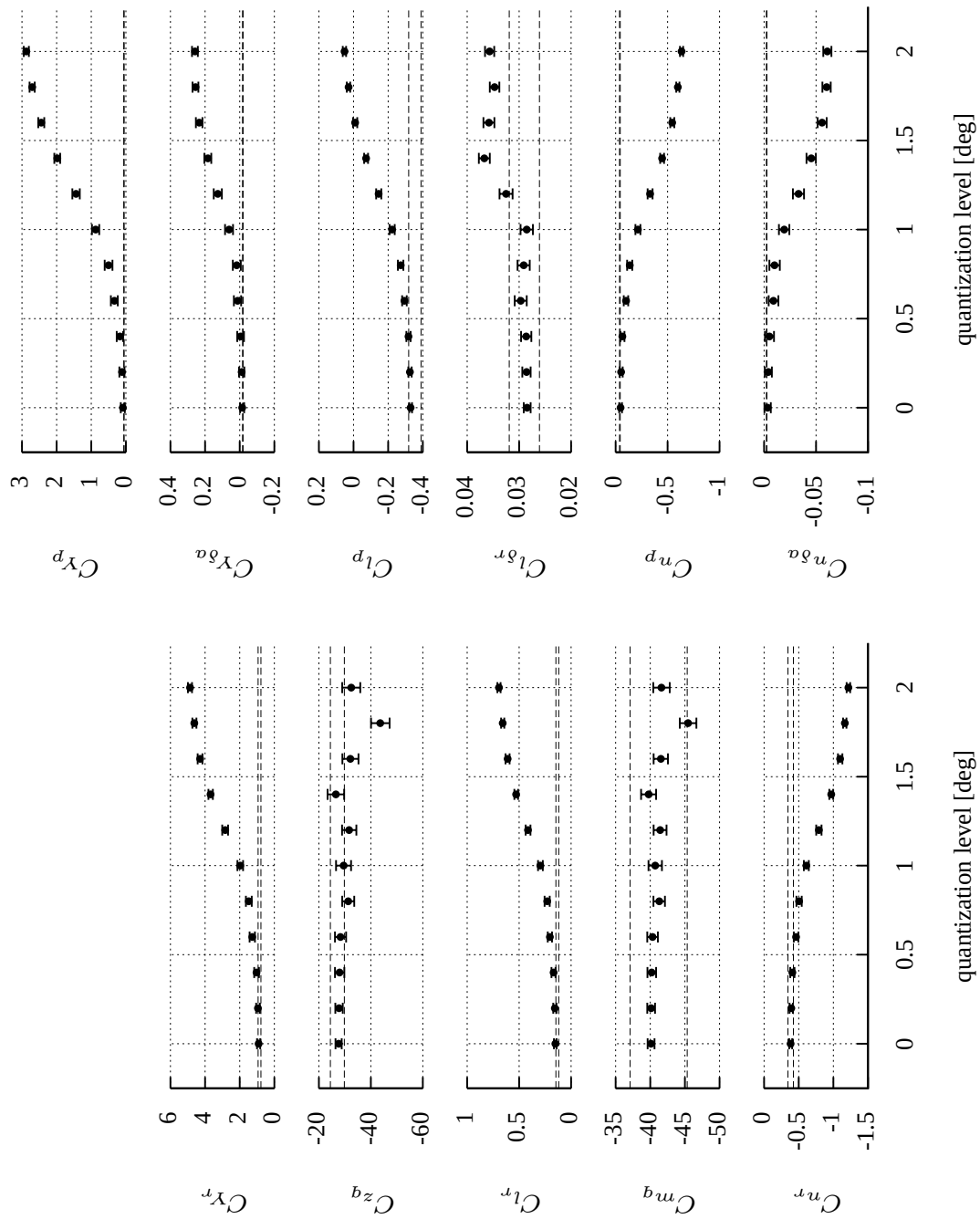

Figure 5. Variation in GTM stability and control derivatives with air flow angle resolution (other derivatives)

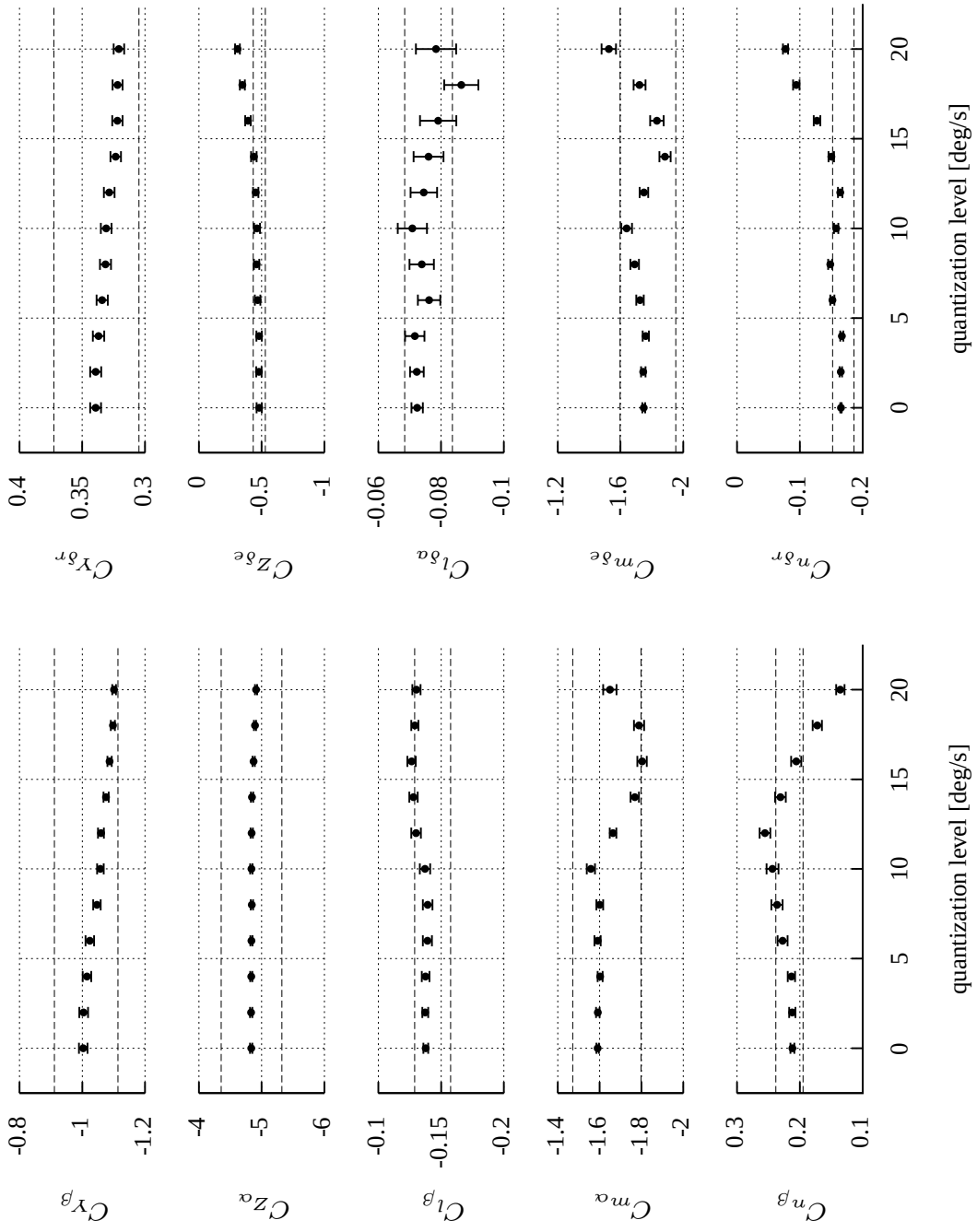

Figure 6. Variation in GTM stability and control derivatives with gyroscope resolution

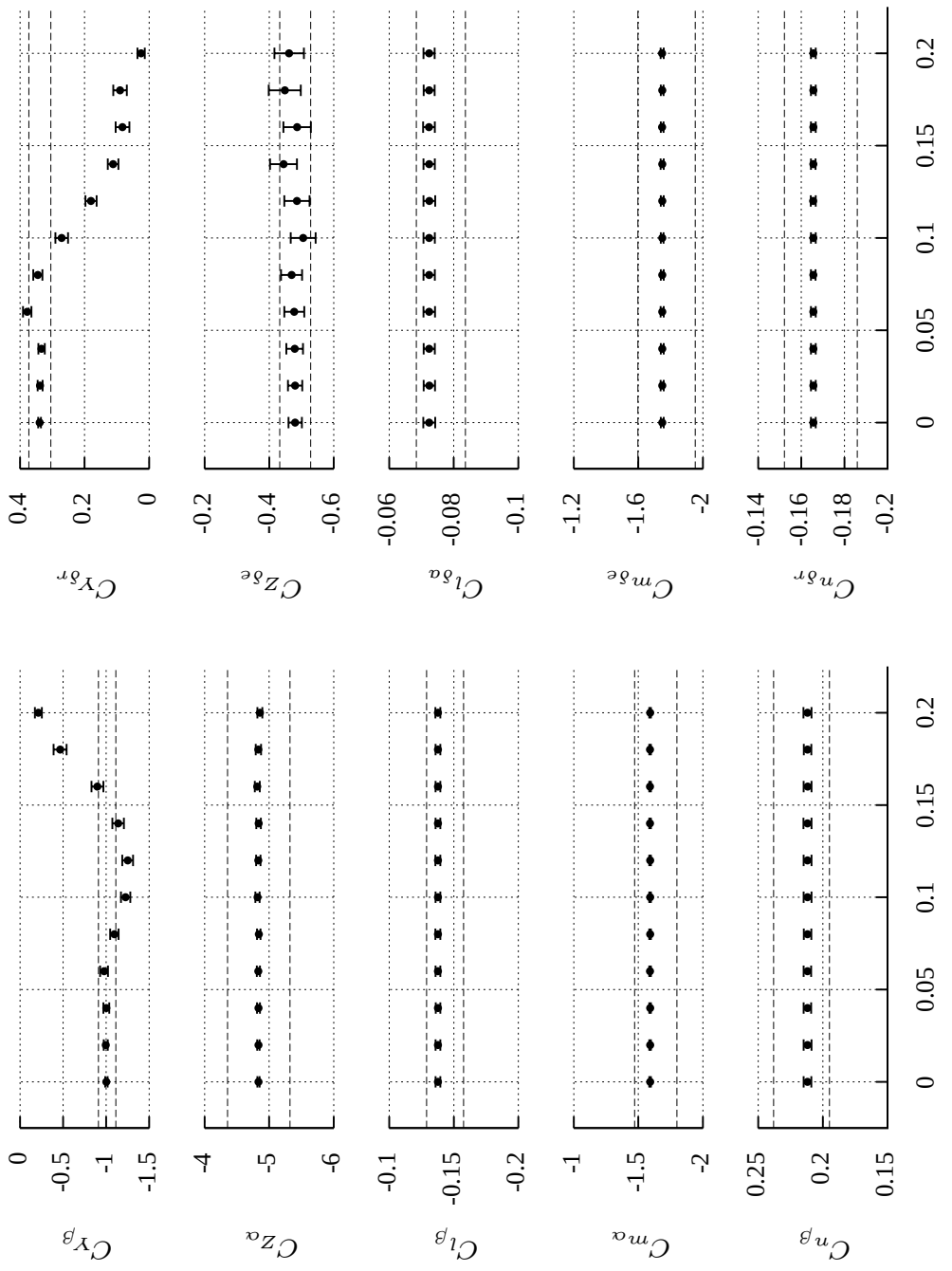

Figure 7. Variation in GTM stability and control derivatives with accelerometer resolution

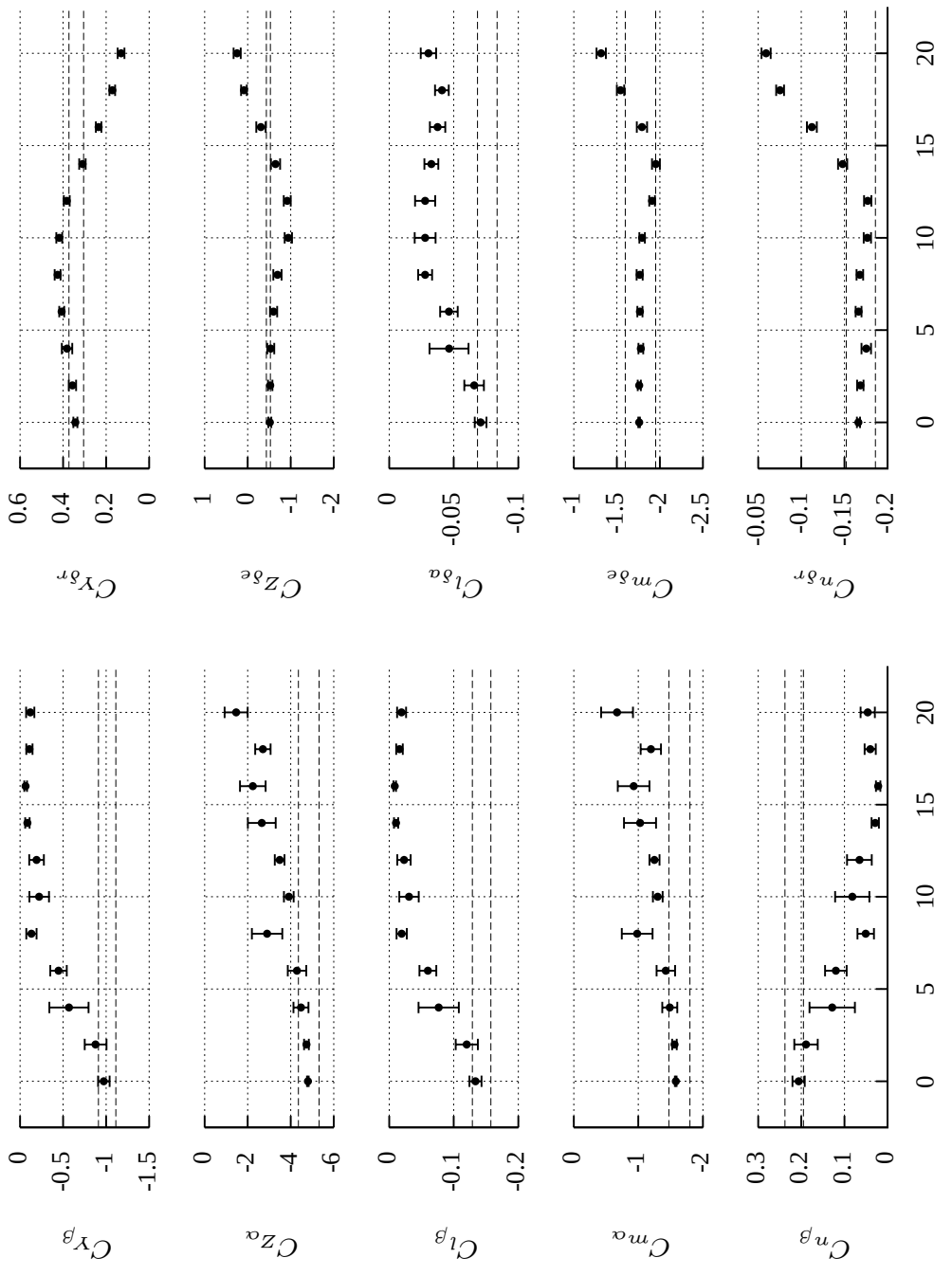

Figure 8. Variation in GTM stability and control derivatives with gyroscope resolution and air flow angle reconstruction

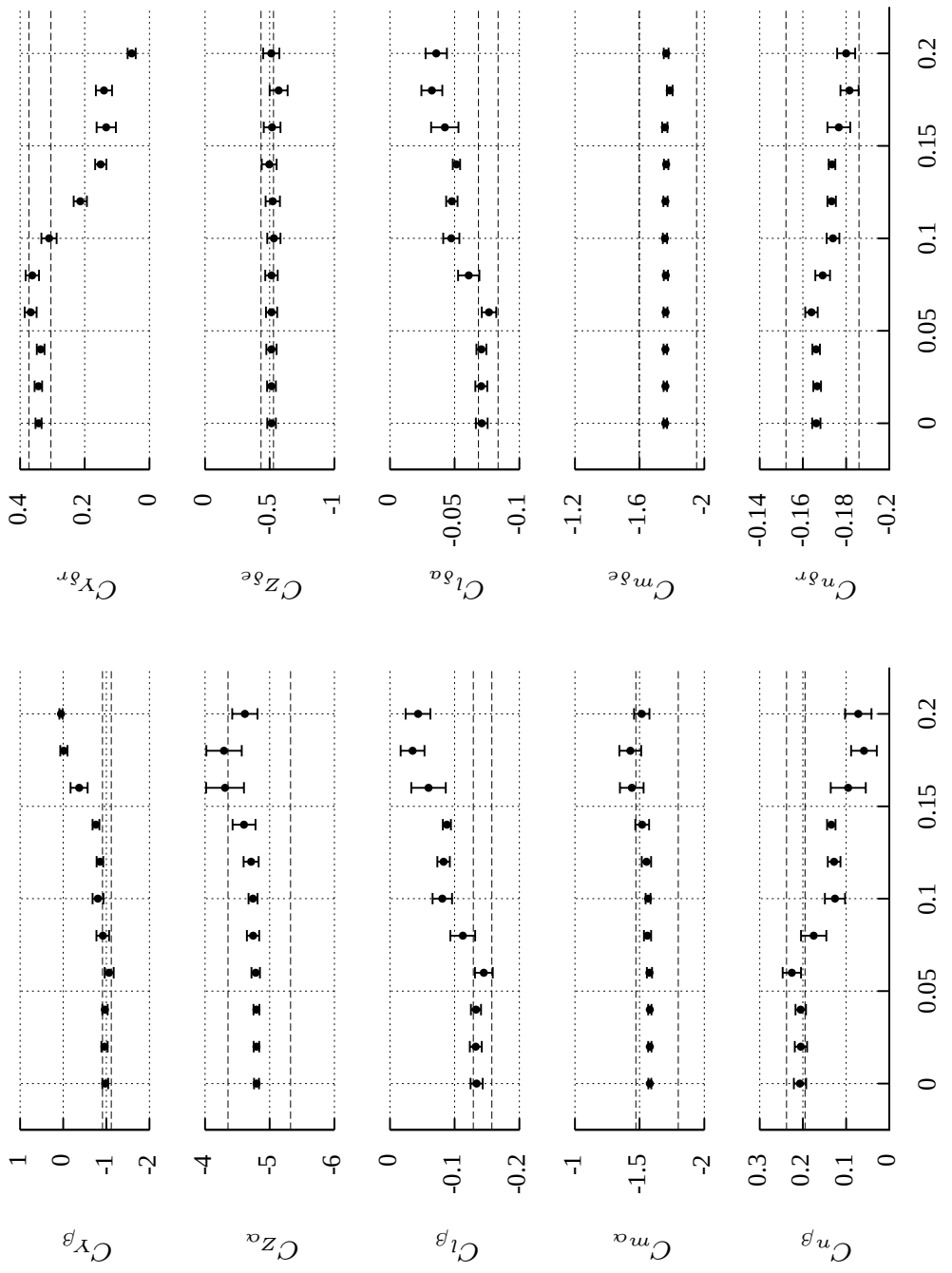

Figure 9. Variation in GTM stability and control derivatives with accelerometer resolution and air flow angle reconstruction

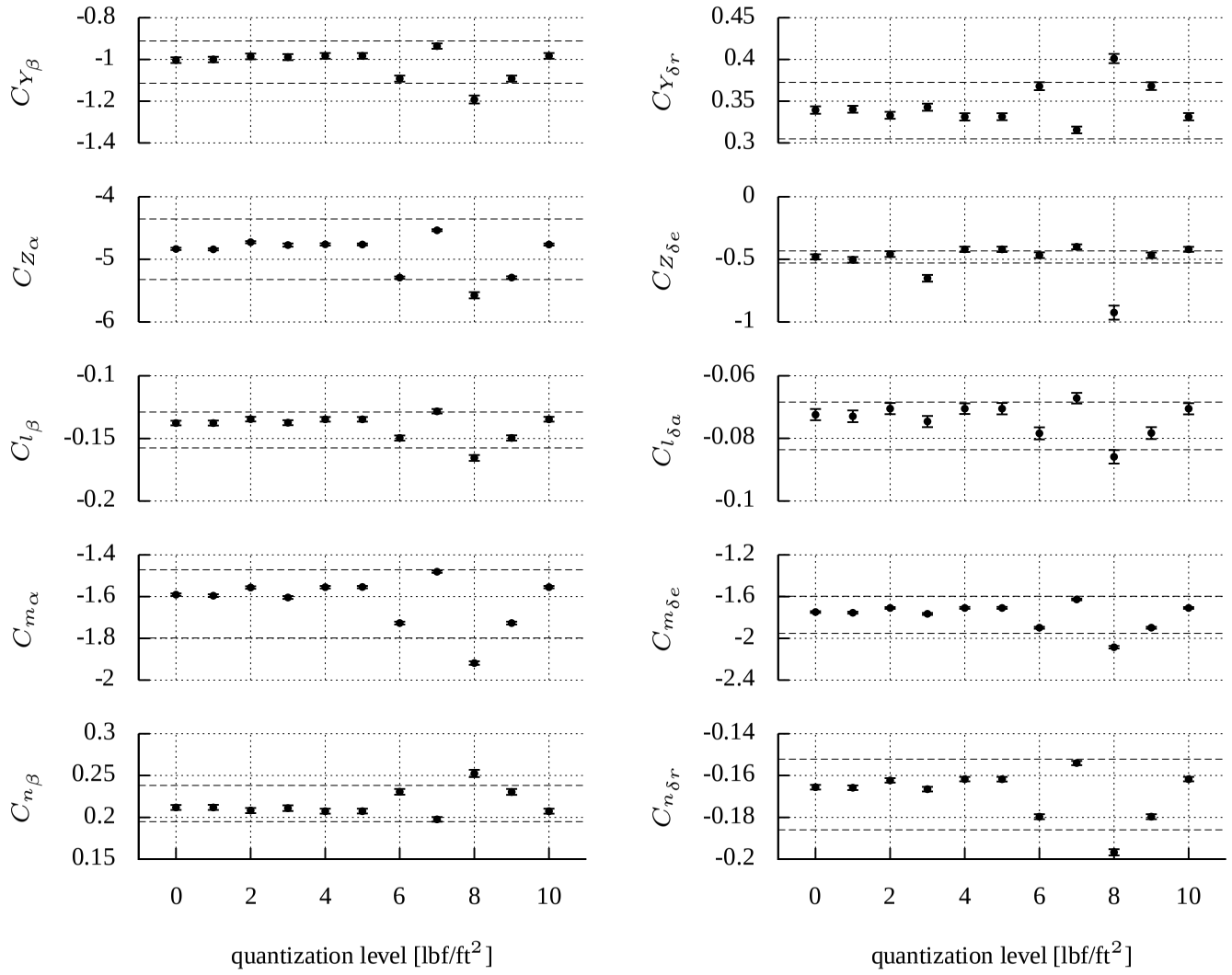

Figure 10. Variation in GTM stability and control derivatives with dynamic pressure resolution

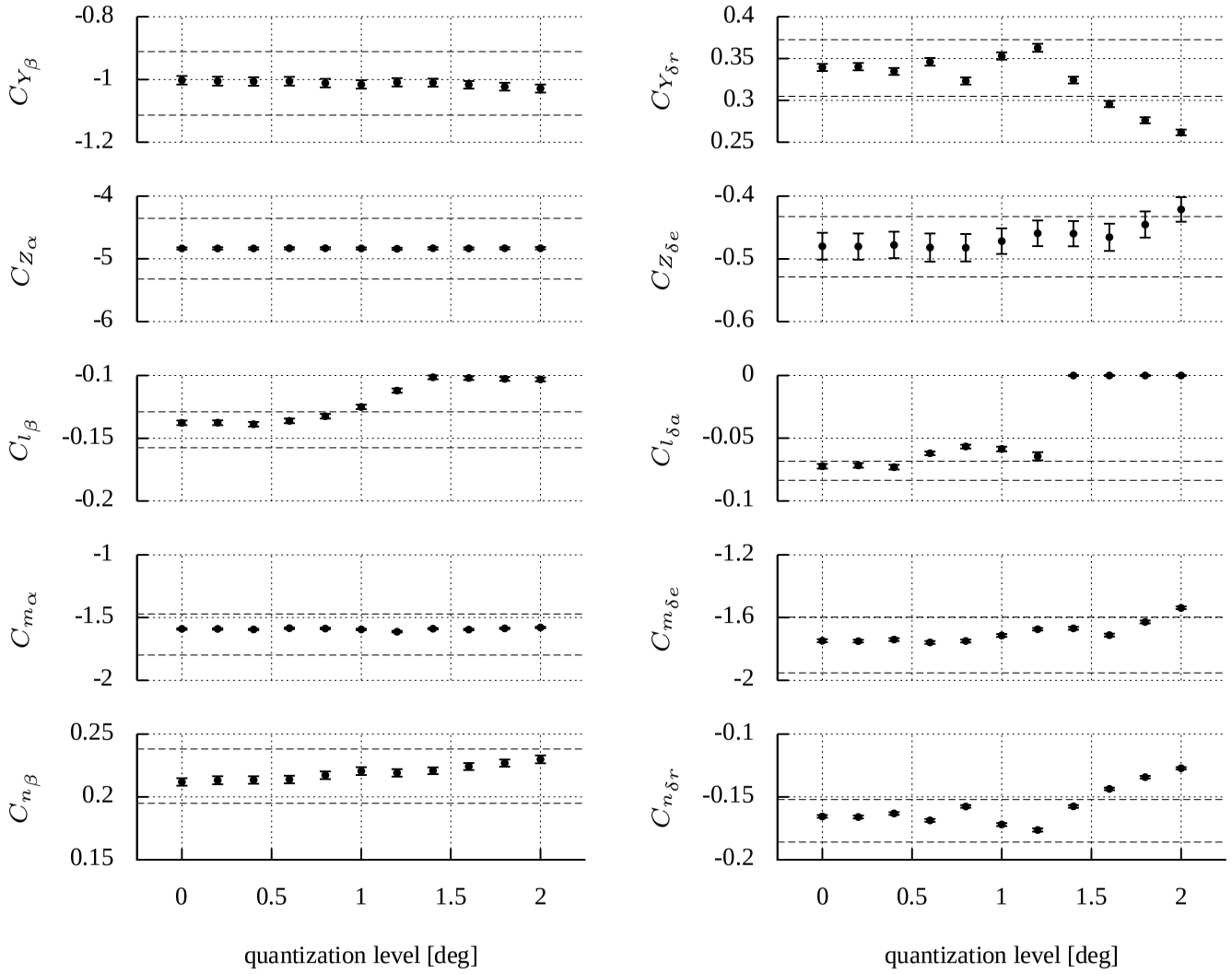

Figure 11. Variation in GTM stability and control derivatives with control surface potentiometer resolution

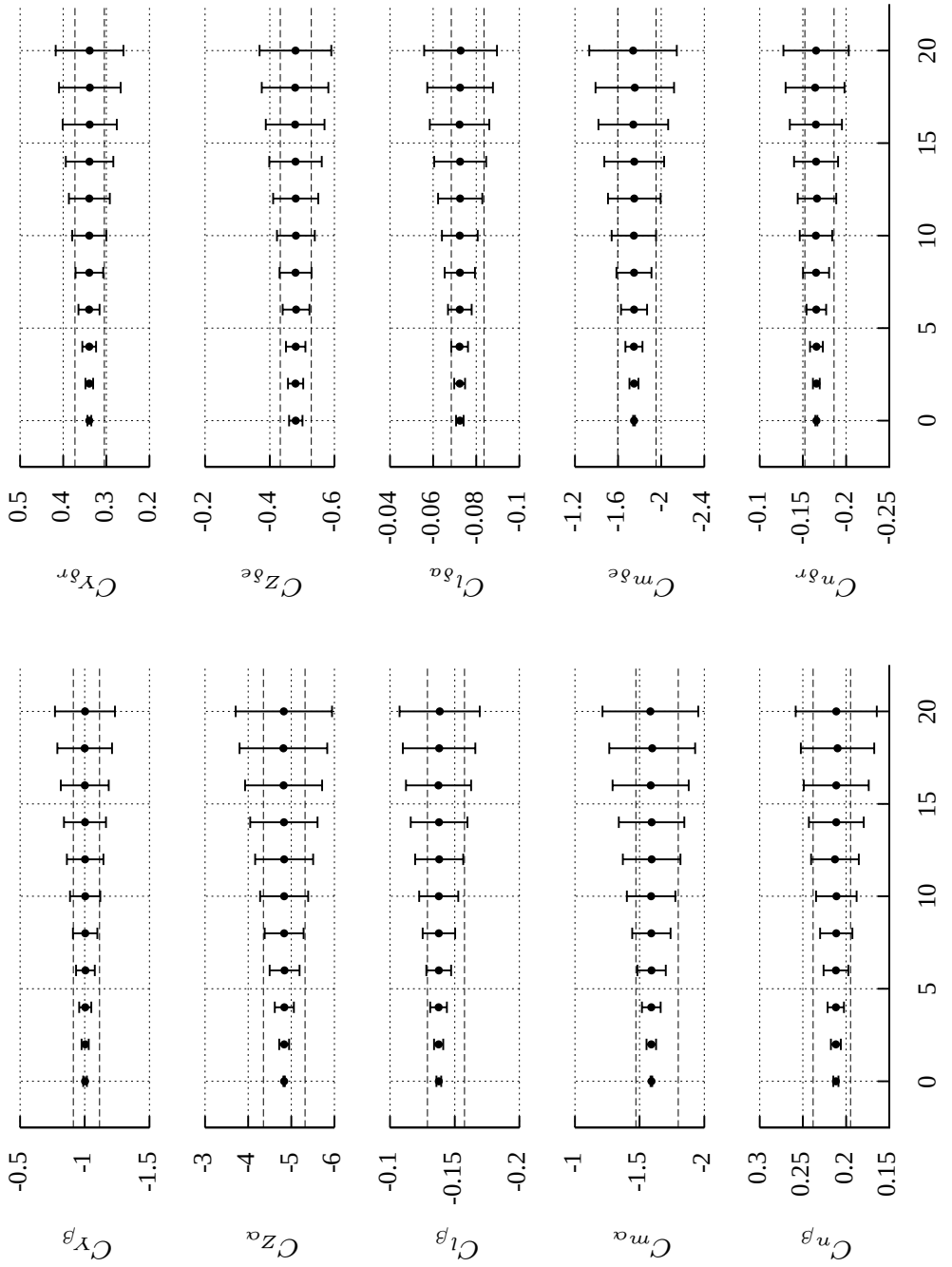

Figure 12. Variation in GTM stability and control derivatives with mass and inertia resolution

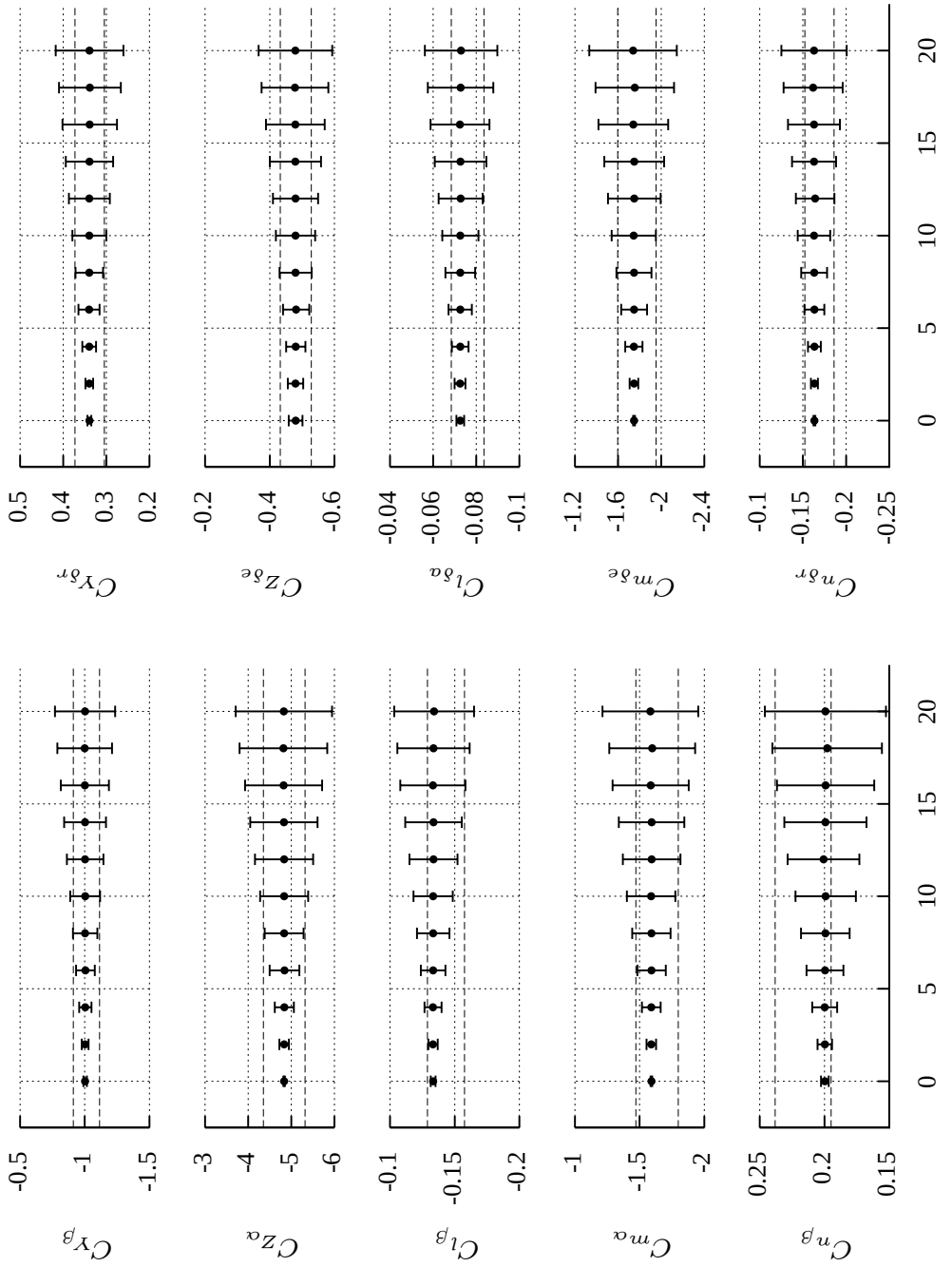

Figure 13. Variation in GTM stability and control derivatives with mass and inertia resolution and negligible I_{xz}

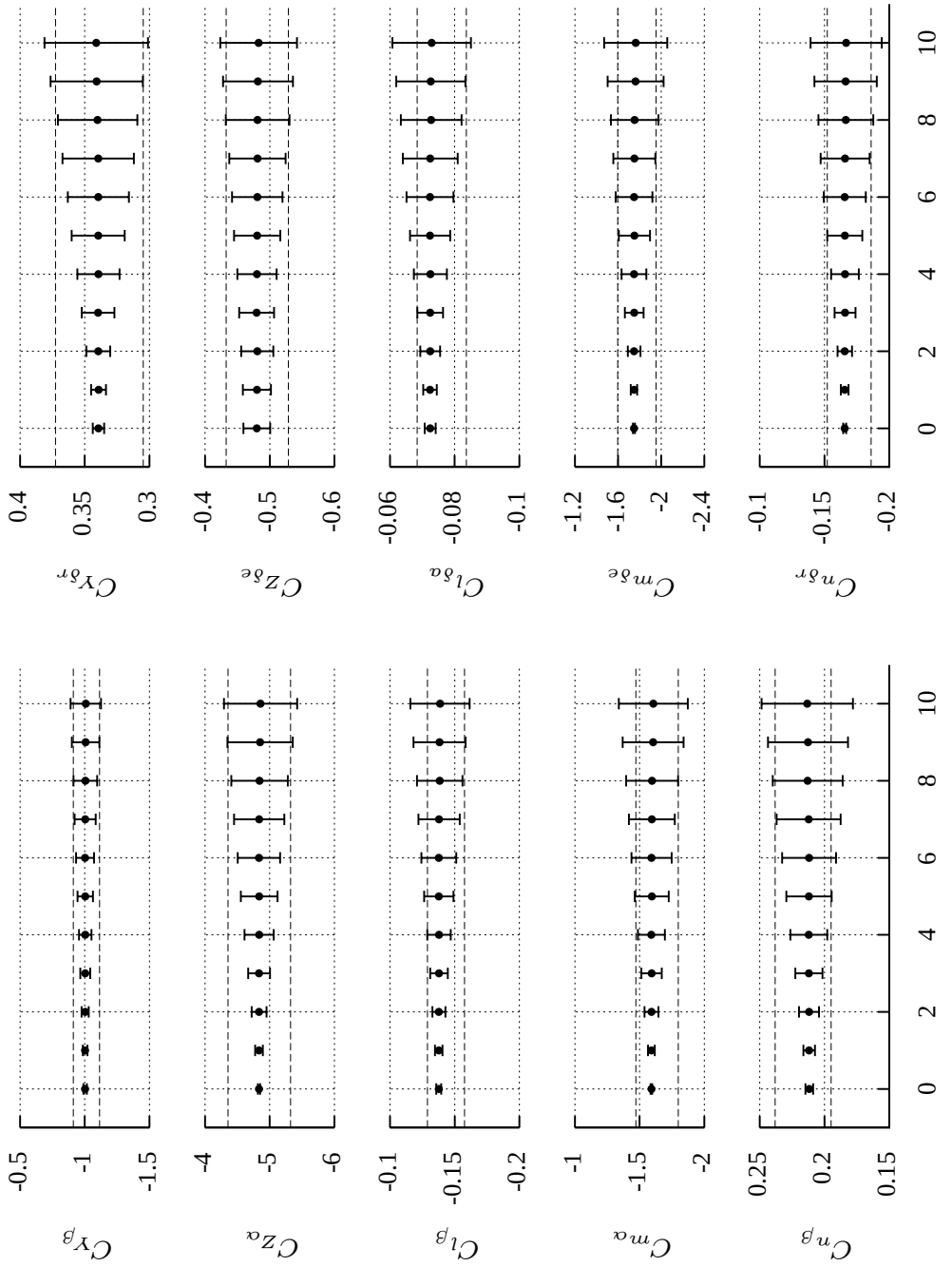

Figure 14. Variation in GTM stability and control derivatives with aircraft geometry resolution

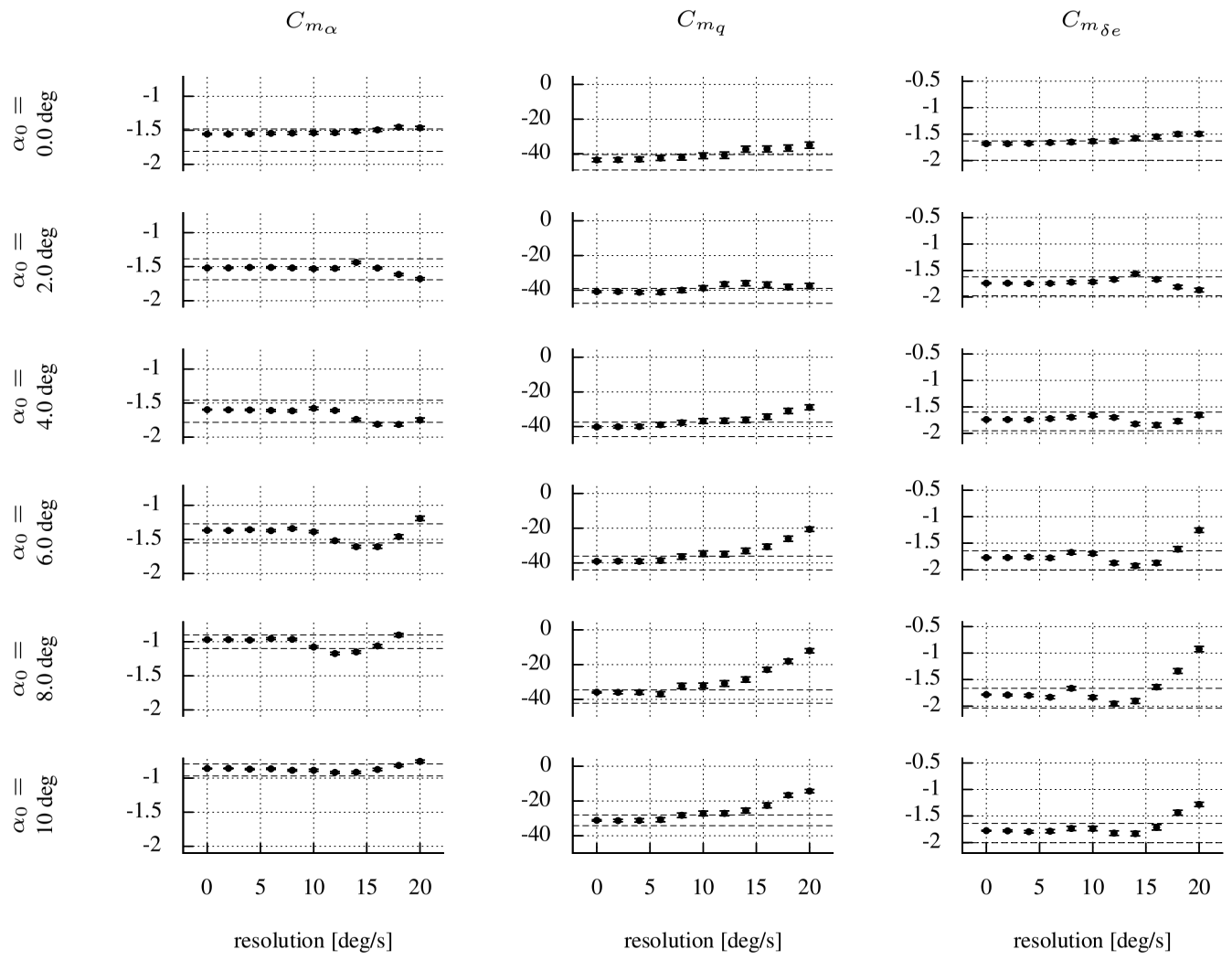

Figure 15. Variation of GTM pitching moment derivatives with varying gyroscope resolution for several trim conditions

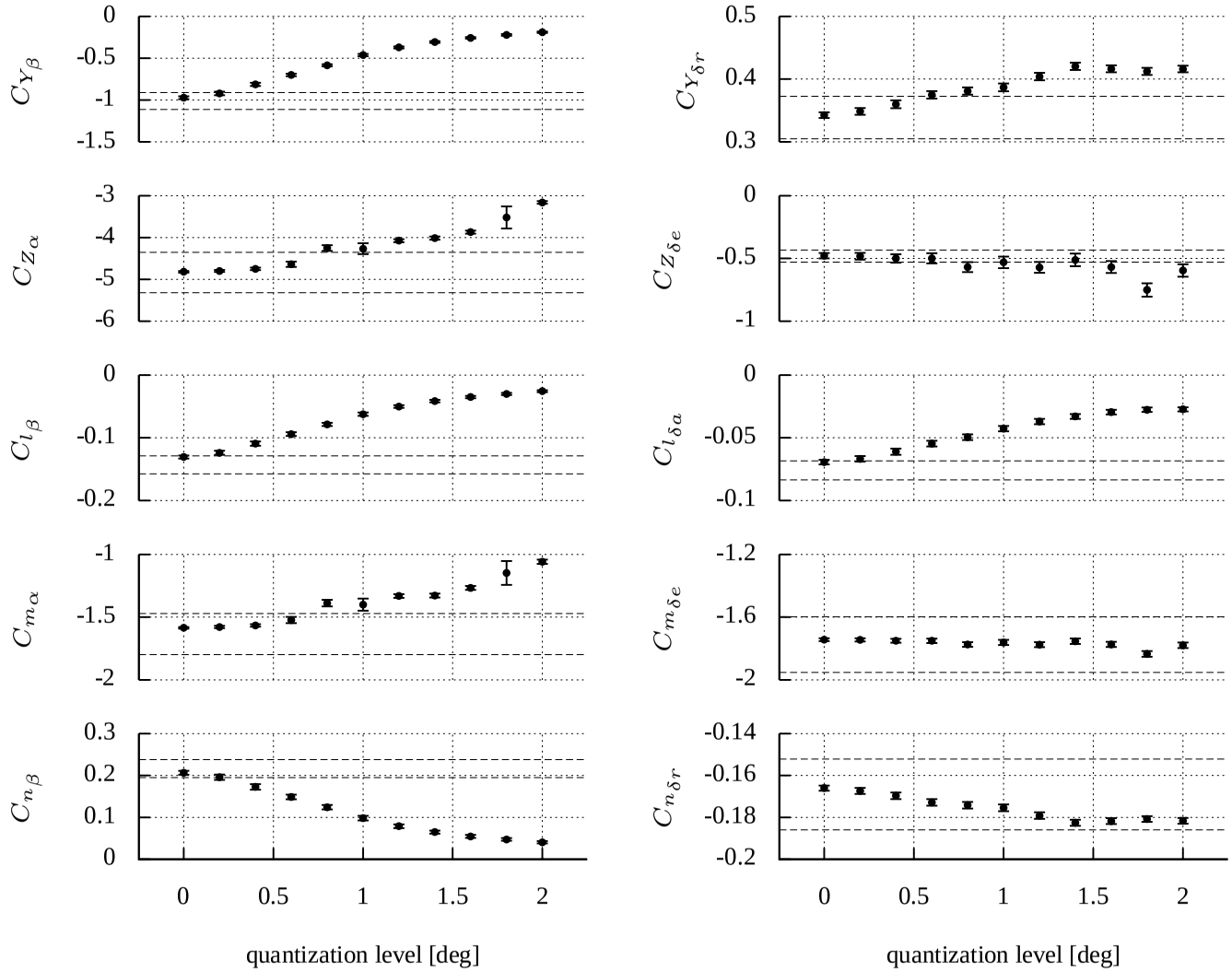

Figure 16. Variation in GTM stability and control derivatives with air flow angle resolution using equation-error parameter estimation in the time domain

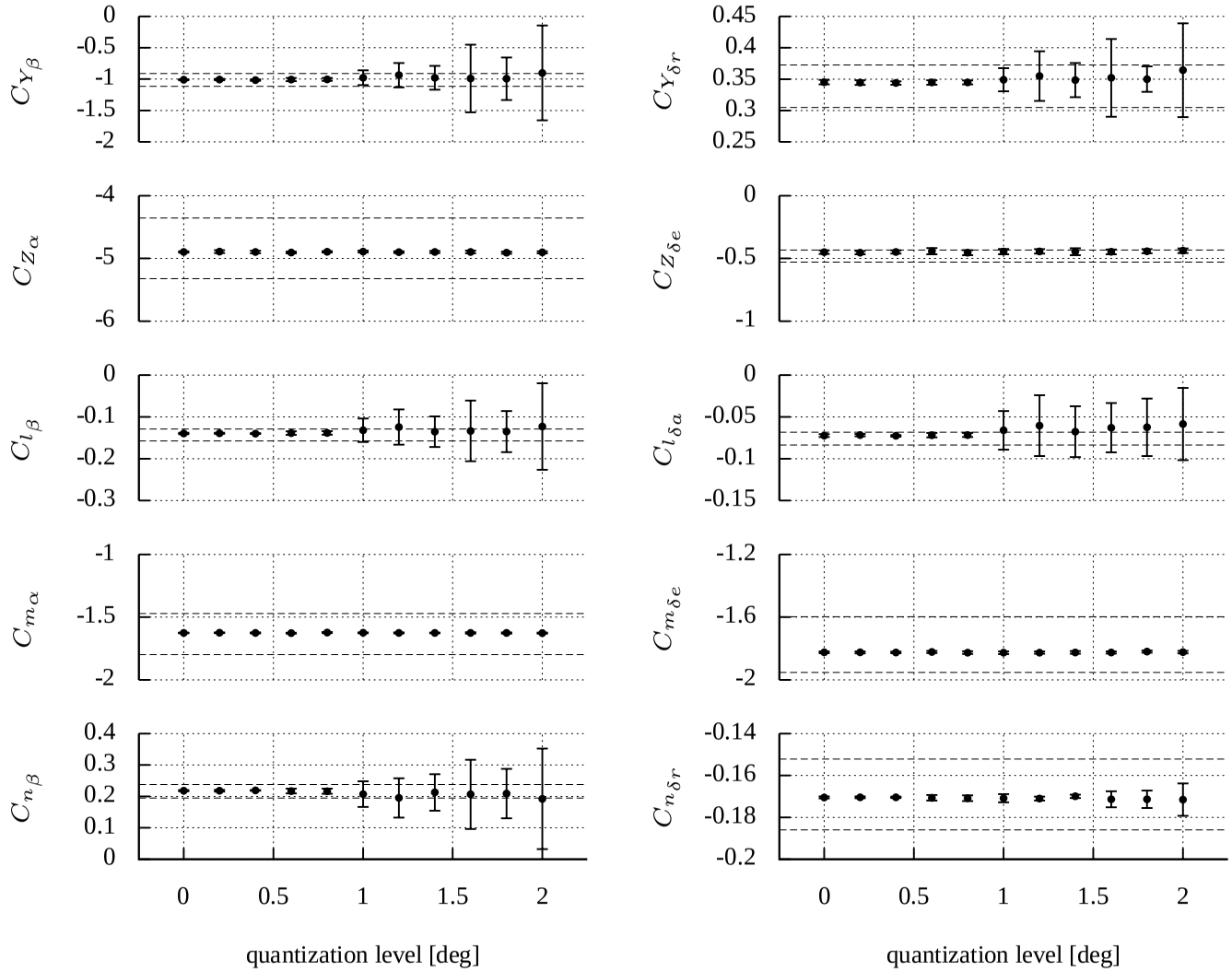

Figure 17. Variation in GTM stability and control derivatives with air flow angle resolution using output-error parameter estimation in the time domain

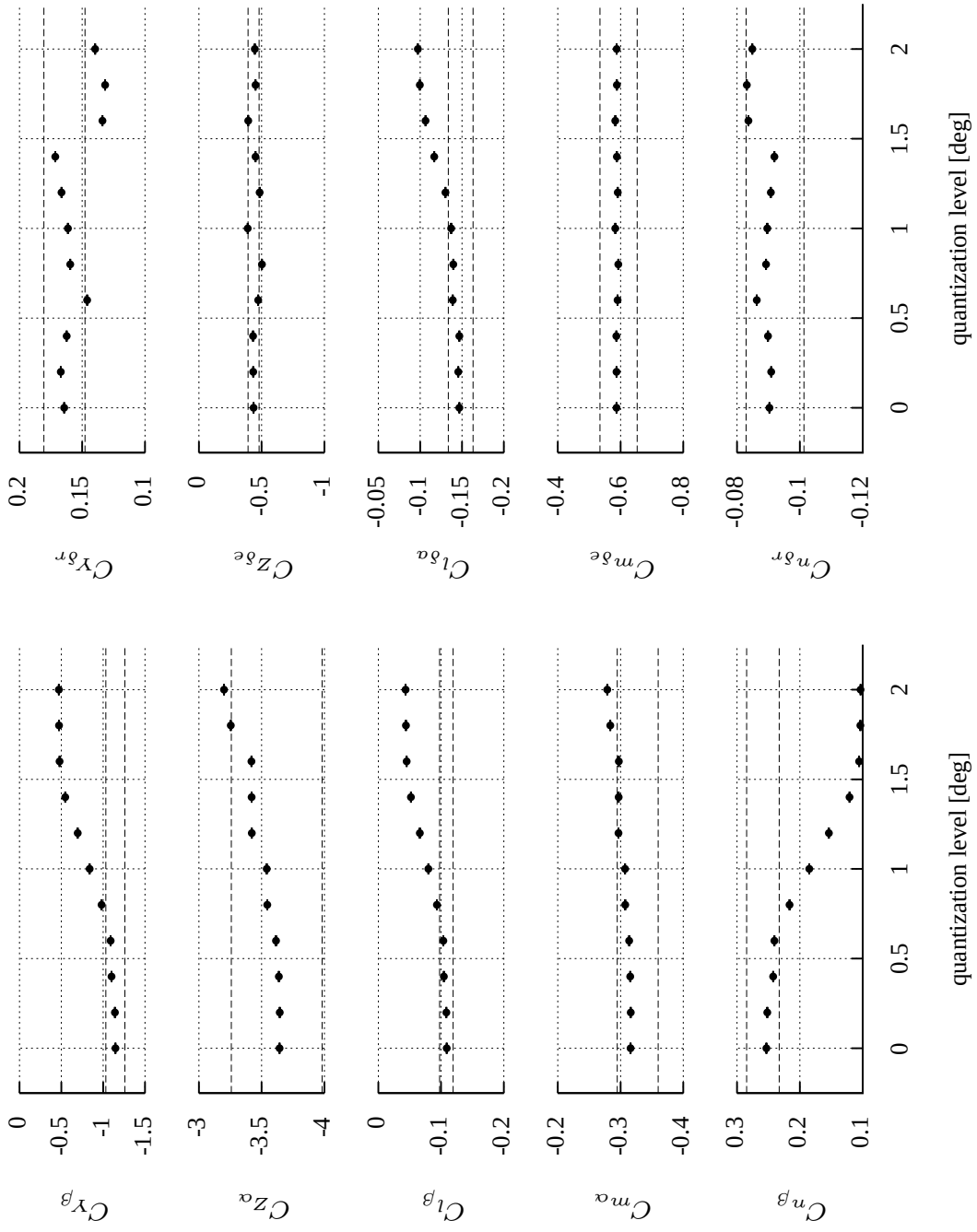

Figure 18. Variation in F-16 stability and control derivatives with air flow angle resolution

REPORT DOCUMENTATION PAGE

Form Approved
OMB No. 0704-0188

1. REPORT DATE *(DD-MM-YYYY)*	2. REPORT TYPE	3. DATES COVERED *(From - To)*
01- 11 - 2013	Technical Memorandum	

4. TITLE AND SUBTITLE

Dependence of Dynamic Modeling Accuracy on Sensor Measurements, Mass Properties, and Aircraft Geometry

5a. CONTRACT NUMBER

5b. GRANT NUMBER

5c. PROGRAM ELEMENT NUMBER

6. AUTHOR(S)

Grauer, Jared A.; Morelli, Eugene A.

5d. PROJECT NUMBER

5e. TASK NUMBER

5f. WORK UNIT NUMBER

284848.02.05.07.02

7. PERFORMING ORGANIZATION NAME(S) AND ADDRESS(ES)

NASA Langley Research Center
Hampton, VA 23681-2199

8. PERFORMING ORGANIZATION REPORT NUMBER

L-20329

9. SPONSORING/MONITORING AGENCY NAME(S) AND ADDRESS(ES)

National Aeronautics and Space Administration
Washington, DC 20546-0001

10. SPONSOR/MONITOR'S ACRONYM(S)

NASA

11. SPONSOR/MONITOR'S REPORT NUMBER(S)

NASA/TM-2013-218056

12. DISTRIBUTION/AVAILABILITY STATEMENT

Unclassified - Unlimited
Subject Category 08
Availability: NASA CASI (443) 757-5802

13. SUPPLEMENTARY NOTES

14. ABSTRACT

The NASA Generic Transport Model (GTM) nonlinear simulation was used to investigate the effects of errors in sensor measurements, mass properties, and aircraft geometry on the accuracy of identified parameters in mathematical models describing the flight dynamics and determined from flight data. Measurements from a typical flight condition and system identification maneuver were systematically and progressively deteriorated by introducing noise, resolution errors, and bias errors. The data were then used to estimate nondimensional stability and control derivatives within a Monte Carlo simulation. Based on these results, recommendations are provided for maximum allowable errors in sensor measurements, mass properties, and aircraft geometry to achieve desired levels of dynamic modeling accuracy. Results using additional flight conditions and parameter estimation methods, as well as a nonlinear flight simulation of the General Dynamics F-16 aircraft, were compared with these recommendations.

15. SUBJECT TERMS

Generic Transport Model; Measurement accuracy; System identification

16. SECURITY CLASSIFICATION OF:			17. LIMITATION OF ABSTRACT	18. NUMBER OF PAGES	19a. NAME OF RESPONSIBLE PERSON
a. REPORT	b. ABSTRACT	c. THIS PAGE			STI Help Desk (email: help@sti.nasa.gov)
					19b. TELEPHONE NUMBER *(Include area code)*
U	U	U	UU	45	(443) 757-5802